Characterisation of extensional faults in carbonate rocks (Suez Rift, Egypt); with particular focus on the role of shale smear

Master of Science thesis

Lillian Elvik

Department of Earth Science

Centre for Integrated Petroleum Research

University of Bergen

April 2012

Acknowledgement

First of all, I would like to thank my supervisors Eivind Bastesen and Atle Rotevatn, for an interesting project, good supervision and helpful input. They have both been great motivators, always with a positive attitude. Thank you for great discussions both in the field and at the university, for giving helpful feedback and thorough proof reading of manuscripts.

I would also like to thank Anette B. Tvedt for giving constructive comments and help to improve my work. Thank you for a great week in Edinburgh on the TSG-conference and for listening to my presentation over and over again during the preparation for the oral-presentation.

I would like to thank my fellow students at geology at the University of Bergen for five great years and unforgettable memories, both at the university, field trips and gatherings outside the university.

I would especially thank my roommates Oda and Heidrun, who have always been very supportive and given me motivating words. I would also like to thank my family who have been patient and supportive during my years as a student. Finally, I would like to thank James, for being very supporting and encouraging and for helping out proofreading my thesis.

Bergen, 27th of April 2012

Lillian Elvik

Abstract

The distribution, composition and flow-properties of fault core and shale smear along faults in carbonate reservoirs is less well understood compared to faults in siliciclastic rocks. This study uses field data to characterize and quantify fault zone properties that are critical for understanding structural heterogeneity in carbonate reservoirs.

The study focus on; (1) variability and co-dependence of displacement, shale smear, fault- thickness, -composition and -geometry; (2) the effect of shale smearing on fault (core and inner damage zone) deformation; and (3) implications for fluid flow in fault zones in carbonate rocks.

The study area is located on the eastern flank of the Oligocene-Miocene Suez Rift and features large extensional fault arrays affecting fine grained carbonates of Upper Cretaceous to Eocene age. This study is based on structural data from two of these faults (3-6 km length; 30 to 550 m throw). The results show variations in the fault core geometry and composition along the faults. Compositionally, the fault cores are comprised of carbonate breccias, shale smear, secondary calcite and host rock lenses. There is also a significant variation in the thickness of shale smear where this is present (up to 2 m thickness recorded). Investigation of the variability of the said fault parameters indicates that the properties of fault core and inner damage zone are affected by the presence or absence of shale smear. Shale smear introduces a weak mechanical layer in the fault, acting as a ”lubricant” or “cushion” during slip. This appears to control the structural style and geometry of the fault core, and have also been observed to affect the inner damage zone in terms of enhanced fracture intensities, where shale smear is absent. In turn, both shale smear, in its own right as well as fault core properties, control the effect of any fault on fluid flow. Thus, the present study contributes new knowledge to fault seal analysis in subsurface carbonate reservoirs.

Table of Contents

1. Introduction

1.1 Background and rationale

Approximately 50% of the world`s oil and gas supply, including some of the largest oil fields in the world, are trapped in carbonate reservoirs (Mazzullo, 2004; Ferrill and Morris, 2008). In the upper crustal regime, the fault zone architecture and the related permeability structures have a major control on fluid flow (Verhaert et al., 2009). To forecast and model the structural heterogeneity of carbonate reservoirs, characterisation and quantification of fault zones in outcrops are critical (Bastesen and Braathen, 2010). Depending on the fault zone properties, fault zones may act as a conduit, barrier or a combined conduit-barrier in relation to fluid flow (Caine et al., 1996; Aydin, 2000). Important fault zone properties include fault thickness, composition, geometry and displacement (Yielding et al., 1997; Wibberley et al., 2008; Braathen et al., 2009). Since seismic resolution normally is inadequate to reveal details about the fault zone architecture and composition (Ferrill and Morris, 2008), studies of outcrop analogues are much needed in order to make predictions of subsurface carbonate reservoirs. Despite the interest for exploration and production in deformed carbonate reservoirs, details of important fault zone properties and their effect on fluid flow remain poorly understood (Ferrill et al., 2011).

1.2 Aims of study

The overall aim of this study has been to attempt to improve the understanding of fault zone architecture and structural style in carbonate-shale sequences. This study will use field data to characterise and quantify the fault zone properties that are critical for understanding the structural heterogeneity of carbonate reservoirs. Specifically, this study aims to establish the; 1) variability and co-dependence of throw, shale smear, fault- thickness, -composition and -geometry; 2) effect of shale smearing on fault (core and inner damage zone) deformation and 3) implications for fluid flow in fault zones.

The field area was shared with another master student, Svein-Martin S. Hatleseth, who has focused on fracture systems in the damage zone surrounding the fault. Descriptions and discussion of the damage zone is therefore in the present thesis limited to structural features occurring immediately outside the fault core (the inner damage zone).

1.3 Study area

The study area of this thesis is located on the eastern flank of the Oligocene-Miocene Suez Rift (Fig.1.1), which is a NW-SE extension of the Red Sea rift system. The Suez Rift system, which is a result of the separation between the Arabian and African plate in Oligocene-Miocene times, features typical rift geometries, including segmented normal fault systems, rotated fault blocks and half-grabens (e.g. Bosworth et al., 2005). The Hammam Faraun Fault Block, where the study area is located (Fig.1.1), is one of the major fault blocks in the central Suez Rift. It forms part of the eastern flank of the rift, and is exposed on the western shores of the Sinai Peninsula (Gawthorpe et al., 2003). The study area (Fig.1.1) offers a superb opportunity to investigate fault zone architecture in pre-rift carbonate rocks of Upper Cretaceous-Eocene age. The area provides exceptional 3D exposures due to the cross-cutting wadi networks (dry river beds) and limited vegetation.

Fig. 1.1: Satellite image of the Sinai Peninsula, Red Sea, Gulf of Suez and Gulf of Aqaba (NasaScienceLibrary, 2012). The study area is located in the central part of the Suez rift.

The Hammam Faraun Fault Block has been the focus of numerous studies focusing on rift evolution, from both a structural and sedimentological point of view (e.g. Moustafa, 1996; Sharp et al., 2000b; Jackson et al., 2002; Gawthorpe et al., 2003; Leppard and Gawthorpe, 2006). However, only a very limited number of studies have focused in detail on the fault zone evolution in the pre-rift carbonates in the area (Bastesen and Braathen, 2010)

Details about the geological framework and the stratigraphy of the area will be presented in more detail in chapter 2.

.

1.4 Concepts and terminology

1.4.1 Fault architecture

Brittle fault zones represent discontinuities in the upper crust that are both lithologically heterogeneous and structurally anisotropic (Caine et al., 1996; Faulkner et al., 2010). Fault zones are generally described by distinct components, such as a fault core, a damage zone and a protolith (Chester and Logan, 1987; Caine et al., 1996), as illustrated in the conceptual model of Bastesen (2010) (Fig.1.2). A fault core (Fig. 1.2) is defined as the area where most of the displacement is accommodated and may include several elements such as slip surfaces, fault rocks, lenses of protolith or fault rock, shale smear and fractures (Chester and Logan, 1987; Caine et al., 1996; Bastesen and Braathen, 2010). The damage zone (Fig. 1.2) bounds the fault core and is a network of subsidiary structures such as small faults, veins, fractures. While almost the entire displacement is localised in the slip zone of the fault, there is only a small amount or no offset in the damage zone (Caine et al., 1996). In this study, the term inner damage zone, adapted from Micarelli et al., (2006), will be used, characterising the inner part of the damage zone which is located closest to the fault core.

Although the descriptive terms fault core and damage zone (Fig.1.2) are widely accepted among scientists, other authors have suggested different descriptions of fault zones. Childs et al. (2009) suggested other components such as fault rock, fault zone and relay zone to describe the architectural elements of a fault zone. In the current study, however, the definition by Chester and Logan (1987) and Caine et al. (1996) will be used since this definition is more applicable in the field and for the purpose of this study. The conceptual model from Bastesen (2010) displays the important elements of fault zones in a carbonate-shale sequence (Fig. 1.2).

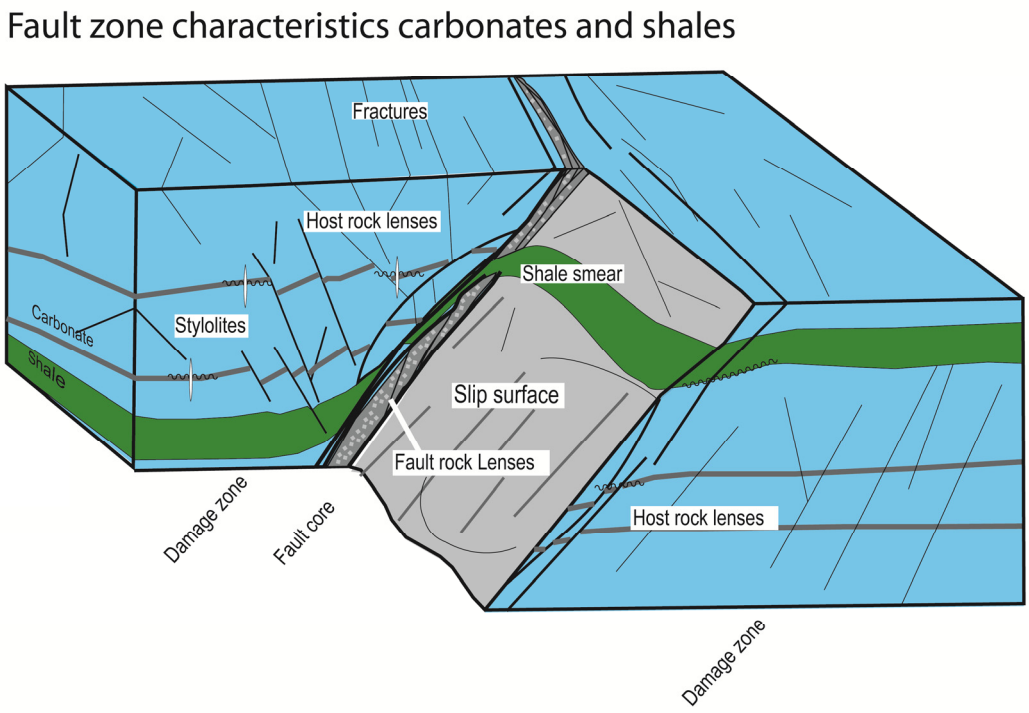

Fig 1.2: Conceptual model of a fault zone in a carbonate-shale sequence displaying important elements related to the fault core and damage zone of the fault (Bastesen, 2010).

1.4.2 Fault rock classification

Fault rocks or fault related rocks are formed by processes involving the crushing of rocks and minerals, and are a result of repeated fracturing, frictional sliding and grinding along one or several faults (Davis and Reynolds, 1996). Lithology, confining pressure, temperature, fluid pressure and kinematics at the time of faulting is factors that determine the type of fault rock (Sibson, 1977). Textures that are preserved in the fault rocks may give valuable information concerning the deformation mechanisms and the structural setting (Sibson, 1977; Braathen et al., 2004). Classification, formation mechanisms and interpretation of fault rocks is a broadly discussed subject and several classification schemes has been made through time (e.g. Sibson, 1977; Wise et al., 1984; Braathen et al., 2004). In the fault rock descriptions in the current study the classification proposed by Braathen et al. (2004) will be used (Fig. 1.3). This diagram is based on existing classification schemes with additional, more precise naming of the different fault rocks after observations made in the field. The classification scheme (Fig. 1.3) is based on which deformation mechanisms were active during the formation of the fault rock and the cohesion of the fault rock after formation. The classification scheme (Fig.1.3) also reflects the amount of matrix, grain size and the amount of phyllosillicate minerals present (Braathen et al., 2004).

Fault rocks such as breccias and gouge are normally non-cohesive immediately after formation, but may appear as cohesive rocks in a fault (secondary cohesion). This secondary cohesion is mainly caused by cementation of the matrix, compaction or re-crystallization (Braathen et al., 2004). Fault rocks such as gouge and breccias are normally the products of brittle deformation in shallow fault zones. This is especially the case if the fault zones are in tight, impermeable, mechanically strong rocks, such as carbonates or granites (Sibson, 1977). Breccias are characterised by angular fragments set in a finer-grained matrix (Davis and Reynolds, 1996).

Deeper into the crust, at the ductile-brittle transition, deformation mechanisms are characterised by granulation, which includes fracturing and frictional gliding. This results in grain-size reduction (Braathen et al., 2004). These conditions are associated with the fault rock cataclasite, which is a rock that has developed with cohesion by mainly frictional flow. These rocks normally have a chaotic texture (Braathen et al., 2004). Fault rocks developed even deeper in the crust, are characterised by plastic flow (Sibson, 1977). Since this thesis only will focus on deformation mechanisms related to brittle deformation, fault rocks related to the plastic regime will not be explained further.

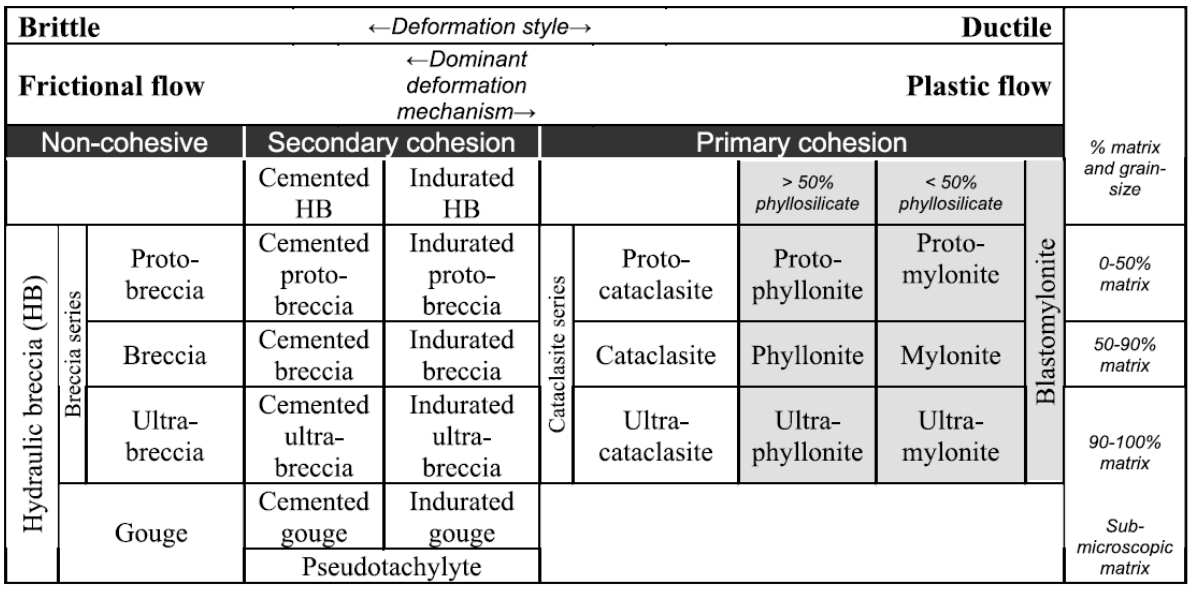

Fig 1.3: Classification scheme by Braathen et al. (2004), where the classification of the different fault rocks are based on deformation style, deformation mechanisms and cohesion. The diagram also differentiates on clast-matrix distribution, grain size and the amount of phyllosilicate minerals.

1.4.3 Shale smear

The process where shale or clay gets entrained into the fault zone during fault movement is called smearing. The term shale smear (Fig.1.4) is often used on this more or less continuous shale membrane, a term which was first used as a general term for shale or clay layers incorporated in a fault between sandstone units (Lindsay et al., 1993). Clay may be secondarily formed in almost any rock type, but the most common source of clay in a fault zone is from the sedimentary sequence itself (Lindsay et al., 1993; Færseth, 2006). Figure 1.4 show a conceptual model of the evolution of shale smear within a fault zone, modified from Færseth (2006). Due to their small pore spaces and pore throats, clay or shale can act as a barrier to fluid flow and prevent fluids from leaking across or along the fault (Færseth, 2006).

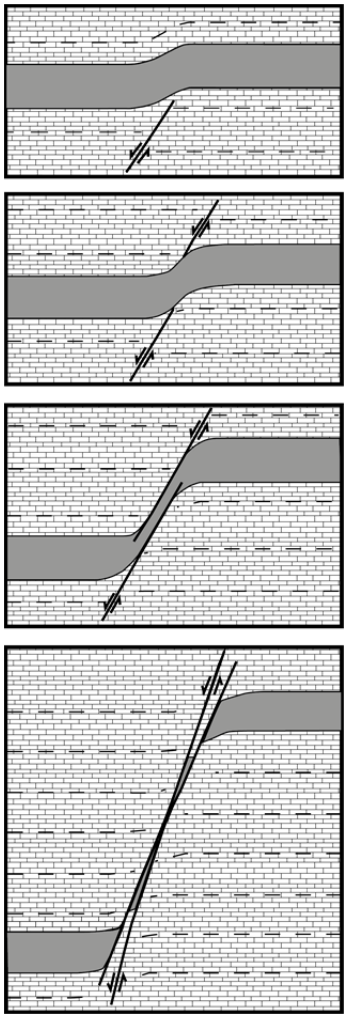

Fig. 1.4: Conceptual model of the evolution of shale smear within a fault zone, modified from Færseth (2006). As the throw increases on a fault, the shale becomes entrained into the fault zone as continuous smear. As the throw increases further, the shale becomes discontinuous.

Being able to predict the presence of shale in the fault is therefore important in terms of fault seal analysis and several authors have suggested algorithms that describe the likelihood of smear within the fault zone. Lindsay et al. (1993) measured the continuity of shale smear along small faults with throw up to 15 meters in sandstone-shale sequences (Lindsay et al., 1993). They introduced the shale smear factor (SSF) to assess the effect of shale smear and to predict shale smear continuity. The SSF is calculated by the throw of the fault divided by the thickness of the shale bed. They concluded that with a SSF ≤7 continuous shale smear is expected, while with a SSF ≤11 continuous shale smear is probable. This definition was later assessed by Færseth (2006), which also included larger (> 60 m throw) faults in both carbonate and sandstone sequences. Based on data from faults offshore from Norway and from outcrops onshore in various study areas, they argue that with a SSF ≤4, continuous shale smear is expected, while with a SSF >6, continuous shale smear is unlikely.

1.5 Methodology

Data used in this study is mainly derived from field work carried out in March and November 2011 in Sinai, Egypt. Traditional field methods have been used, including basic geological mapping in combination with quantitative morphological and geometric descriptions of the studied fault zone.

To better assess the deformation processes in the fault zone, a number of localities along the fault were chosen for a detailed study of both the fault core and inner damage zone. To describe the locality properly, images were used to make the recordings easier and more exact. By using tracing paper on the image, the details of the fault zone were recorded. The fault core was logged and the fault rocks present were classified after Braathen et al., (2004) classification scheme. The intensity of veins of calcite and gypsum was also described. Measurements of the orientations of the slip surface, fractures and bedding along the fault were collected. The measurement was recorded using the right hand rule.

To be able to measure the throw of the fault, the local stratigraphy was logged in order to obtain the thickness and the lithology of the faulted units. The purpose of the mapping was to get a better overview on the rock formations in the area, to better understand the structural features formed in the fault zone and to generate meter-scale throw profiles along fault traces.

A wide range of rock samples were collected, from both the fault core and inner damage zone. Polished thin sections were prepared from many of these samples to better characterize the composition of the fault rocks and fault related rocks. This includes diagenetical elements (cement and clay), micro texture and micro tectonic structure.

Fracture analysis was carried out in order to quantitatively define the characteristics of fracture networks affecting the fault core and inner damage zone. The technique used consisted of measuring fractures along scan lines orienting as perpendicular as possible to the strike of the fault, in order to record the changes in fracture intensities. Characteristics such as type of fracture (joints or veins), length, mode, composition of fracture fill were recorded. The orientation of the fractures was also measured.

2. Geological framework

2.1 Regional tectonic framework

The Suez Rift is a rift basin, located between the African and Arabian plates. The rift system, the aborted arm of the Cenozoic Red Sea Rift, is about 300 km long and 80 km wide (e.g. Lyberis, 1988; Bosworth et al., 2005). The NW-SE trending arm was formed as a response to the late Oligocene-Early Miocene rifting of the African and Arabian plates, abating around the time when continued extension within the Red Sea Rift was accommodated by the movement on the Dead Sea-Aqaba transform (Cochran, 1983). Large scale normal faults on both margins define a classic half-graben system with tilted fault blocks (Patton, 1994; Jackson et al., 2002; Gawthorpe et al., 2003). The change in dip direction along the fault axis divides the rift into three different dip-provinces (Patton, 1994; Moustafa, 1996). Normal faults in the northern- and southern dip provinces dip dominantly to the northeast, whilst at the central dip province, the faults dip dominantly to the south-west. The different dip provinces are separated by rift-transverse accommodation zones (Patton, 1994). The dominant rift-parallel faults strike NW-NNW (Sharp et al., 2000a). The Hammam Faraun Fault Block (Fig. 2.1), where the study area is located, is c. 20 km wide and c. 40 km long and lies within the central dip province (Moustafa and Abdeen, 1992). The east-dipping fault block is bounded by the southwest-dipping Hammam Faraun Fault (part of Coastal Fault Belt) to the west and the southwest-dipping Thal Fault (part of Eastern Boundary Fault Belt) in the east (Moustafa and Abdeen, 1992). The Hammam Faraun Fault and Thal Fault are > 25 km long and have a displacement up to 5 km and 2 km respectively. While the dominating fault strike of the border faults is NW-SE, subordinate N-S- , NNE-SSW- and E-W- trending segments create a zigzag pattern in plan view (Gawthorpe et al., 2003). In the Hammam Faraun Fault Block (Fig. 2.1), a series of intra block fault zones is located with displacement up to 1 km with a similar zigzag pattern as the border fault zones.

2.2 Stratigraphic framework

The stratigraphy in the area is often grouped into three main stages following the tectonic evolution of the rift (Fig. 2.2); pre-rift (Cambrian to early Paleogene), syn-rift (Oligocene-Miocene) and post-rift (Post-Miocene) (Moustafa and Abdeen, 1992). The major events and the most important formations will be presented in the next section.

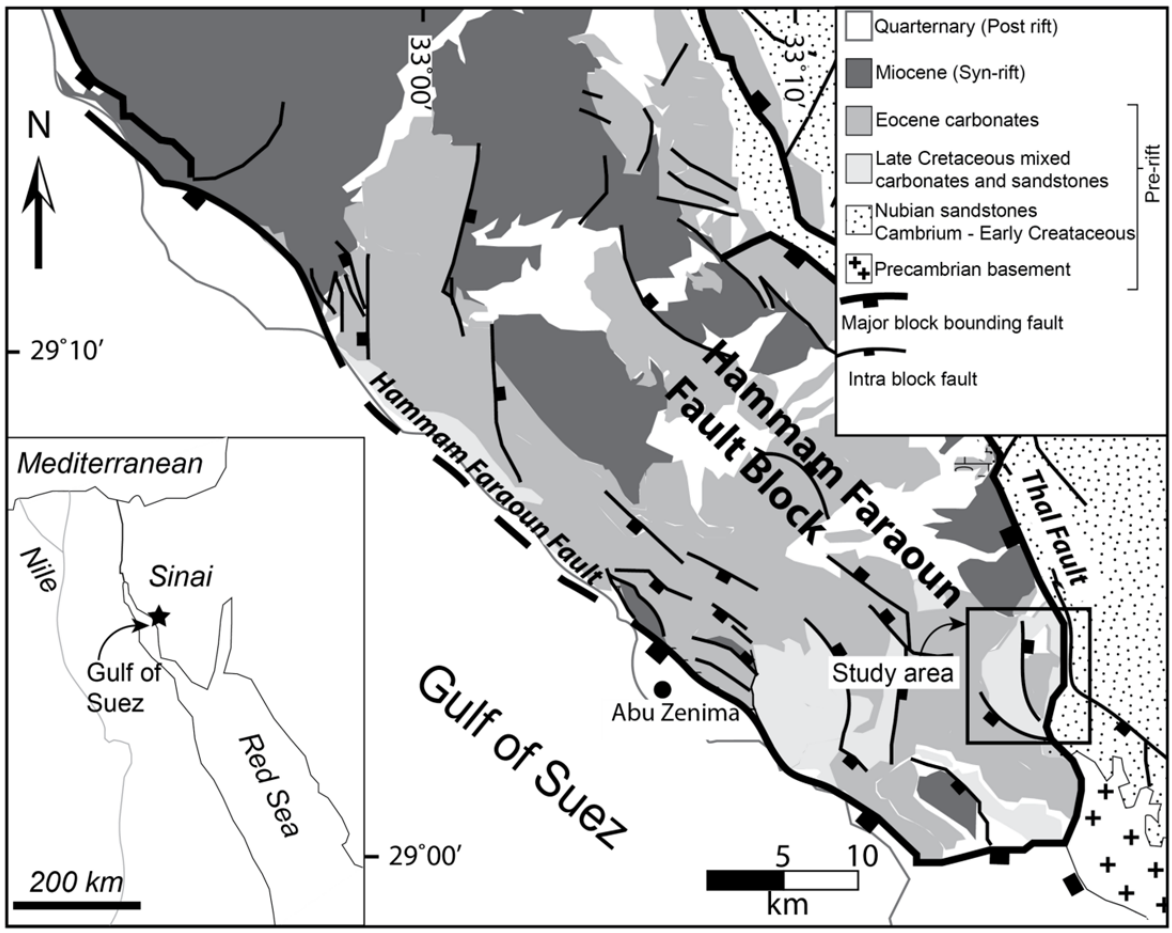

Fig. 2.1: Simplified geological map of the Hammam Faraun Fault Block in Sinai, Egypt modified from Bastesen and Rotevatn (in press). The location of the study area is marked with a black square. A simplified stratigraphic column is showed in the corner of the map.

2.2.1 Pre-Rift

The pre-rift succession is divided into basement rocks and overlying sediment successions of Cambrian to Eocene age. The basement rocks in the Gulf of Suez rift is part of the Arabian-Nubian shield, which is continental crust formed during the Pan-African event, where there was accretion of several intra oceanic island arcs (Patton, 1994). These units are of Precambrian age and consist of igneous and metamorphic rocks of Proterozoic to Lower Paleozoic age (Moustafa, 2004).

From the Cambrian to early Cretaceous, a thick succession of continental silisiclastics was deposited, called the Nubian sandstones (e.g.Gupta et al., 1999) (Fig.2.2). The succession consist predominantly of sandstone sequences, but with a few exceptions of shale and carbonate intervals (Patton, 1994). During the late Cenemonian, a marine transgression occurred, initiating a period of dominantly marine deposition in the Gulf of Suez, which continued until the late Eocene (Moustafa, 2004).

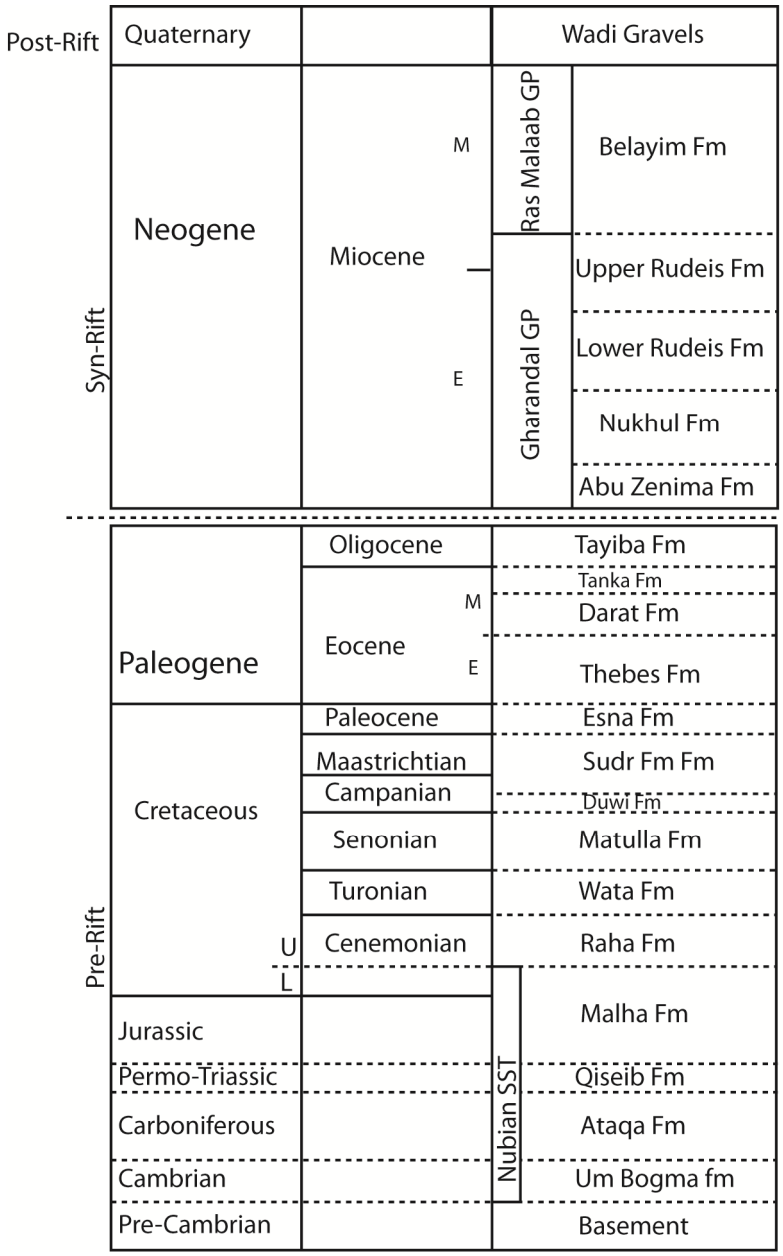

Fig. 2.2: Stratigraphic column showing the formations present in the Hammam Faraun Fault Block, western Sinai, modified from Jackson et al. (2006b). The important formations for this study are of Campanian-Eocene age.

The middle-late Cretaceous (Fig.2.2) is dominated by marine mixed siliciclastics and carbonate deposits of the Raha, Wata, Matulla and Duwi formations (Moustafa, 2004).The main carbonate package in the area and the most important formations for this study are the Upper Cretaceous-Eocene rocks. This is the uppermost and youngest part of the pre-rift package. The Sudr Formation (Maastrichtian age) consists of massive chalky limestones, bedded chalky limestones and chalks (Samuel et al., 2009) The formation is rich with micro fossils, such as planktic foraminifera. The formation was deposited in a warm water, deep marine environment (Samuel et al., 2009). Overlying the white chalk rest the Esna Shale

which is of Late Paleocene to Early Eocene age (Patton, 1994). After reaching its maximum extent in the Upper Cretaceous, the Neo-Tethyan Ocean started closing in the Upper Cretaceous. During this stage, the Syrian Arc fold develops (Moustafa, 1993). The folds follow an ENE-ESE trend across the northern Gulf of Suez and northern Sinai. The thickness of the Esna shale decreases towards the north. This is explained by tectonic movements of the Syrian Arc deformation (Patton, 1994).

The Thebes formation, which conformably overlays the Esna Formation, is comprised of micritic limestone interbedded with chert bands. In the northern part of the Suez rift, this unit is characterized by major slope breccias and slump deposits, probably affected by uplift during Syrian Arch deformation (Kuss, 2000). The Thebes Formation in the study area is characterised by deep marine slope deposits (Kuss, 2000; Scheibner et al., 2000). The Darat and Kaboba formation, of middle Eocene age, consist of limestone interbedded with shale and marl (Patton, 1994). Late Eocene and the latest part of the pre-rift succession are represented by the Mokattam, Tanka and Maadi Formation. While the Mokattam and Tanka Formations consist of mainly densely bedded fossiliferous limestone, the Maadi Formation, also known as the Tayiba Formation in Hammam Faraun area, consist of red to brownish claystone with some limestone ledges (Moustafa, 2004).

2.2.2 Syn-Rift

The earliest evidence for rifting in the Gulf of Suez is represented by the Abu Zenima Formation, which consists of red, purple and varicoloured siltstone, mudstone and sandstones (e.g.Garfunkel, 1977; Gupta et al., 1999). The formation is thought to have been deposited in isolated depocenters during the initial rift sag, in Oligocene-Miocene (Patton, 1994; Jackson et al., 2002). The Oligocene to Early Miocene magmatic phase also provides evidence for the onset of rifting in the area, and consists of basaltic dikes, sills and flows (Moustafa, 2004).

The main syn-rift period is marked by the Early Miocene Nukhul formation (Gupta et al., 1999). The boundary between the Abu Zenima Formation and the overlying Nukhul Formation is associated with a transgressive surface (Jackson et al., 2002). The unit is associated with several facies, ranging from fluvial and shallow marine clastics, to limestones and anhydrites deposited in shallow and open marine environments (Patton, 1994). The top of the Nukhul Formation is marked by a significant depositional hiatus, separating the shallow marine deposits of the Nukhul Formation from the deep water overlying Rudeis Formation. Some authors have argued that this hiatus marks a period with accelerated rifting and an increase in subsidence during this period (Patton, 1994; Young et al., 2002).

The boundary between upper and lower Rudeis is an unconformity called “mid-Rudeis” unconformity, which is thought to be the result of a regional tectonic event which occurred at 17 Ma, and caused uplift of the basin (Young et al., 2002). This is suggested to represent a point where faulting slowed or stopped (Patton, 1994). The rest of the syn-rift period is represented by sandstones of the Kareem Formation (middle Miocene) and the evaporites of the Ras Malaab Group (middle-late Miocene). The presence of the thick evaporites in the upper part of the syn-rift succession is one of the primary obstacles in terms of exploration in the Gulf of Suez, obscuring the seismic images of the underlying pre-rift strata and creating seismic multiples (Patton, 1994). The Ras Malaab group represents a period where there was a decrease in subsidence and the onset of the abandonment of the gulf as a site of active extension.

2.2.3 Post rift

The post rift stage in the Gulf of Suez is represented by Pliocene to Quaternary sediments (Fig.2.2). Although they are referred to as post-rift sediments, there is evidence of fault movements which suggests that rifting continued during their deposition (Bosworth et al., 2005). The quaternary sediments (Patton, 1994) consist of wadi alluvium, windblown sand, terraces, sabkha and reefs

3. Field data

3.1 Introduction

Recent studies in the area have focused on the Nukhul fault strand, which is part of the large Thal Fault (Young et al., 2000). Despite the proximity and association with the Thal Fault, neither of the faults studied herein have previously been described in detail. The purpose of this chapter is to give a detailed description of the faults studied, focusing on geometry, architecture and composition of the fault core and inner damage zone. The study area, shown in figure 3.1a, offers great exposures on fault zone evolution in a carbonate-shale sequence. A general description of the geology in the area will be given at the start of this chapter, focusing on both the structures and the stratigraphy (section 3.2 and 3.3). A wide range of localities was studied in order to give a detailed description of the fault zone. These will be presented in section 3.4. A secondary objective of this thesis is also to calculate a shale smear factor for the studied fault zone; this is addressed in section 3.4.5.

3.2 Structural framework of the study area

The focus of this study has been two intra-block faults within the Hammam Faraun Fault Block. The faults (Fig. 3.1b), which range in length from approximately 3 - 6 km and throw values from 30 to almost 600 m, represent antithetic and synthetic splay faults of the block bounding fault, which in this context is the Thal Fault, dipping to the SW (Sharp et al., 2000a). The Thal Fault is part of the Eastern Boundary Fault Belt and has a displacement of up to c. 2 km. The Thal Fault is approximately 30 km in map view and is defined by rift-parallel fault strands that are linked by shorter, oblique faults (Young et al., 2003). Observations made by Young et al. (2002) indicate that the Thal Fault consist of at least four hard-linked fault strands, namely the Gushea, Abu Ideimat, Sarbut El Gamal and Nukhul fault strands. The centres of the fault strands have the highest fault throw, while the boundaries have the lowest. The studied faults (Fig. 3.1b) are located in the hanging wall of the Thal Fault, and will in this thesis be given the informal names Gebel Nukhul Fault 1 and Gebel Nukhul Fault 2 (GNF1 and GNF2 respectively), named after the close lying mountain, Gebel Nukhul. The geological map of the study area is shown in figure 3.1b, an area of about 20km^2. The map is based on field mapping, existing maps of Moustafa (2004) and satellite imagery from Google Earth. As the map indicates, the localities chosen for this study are mainly located along GNF1 (Fig. 3.1b).

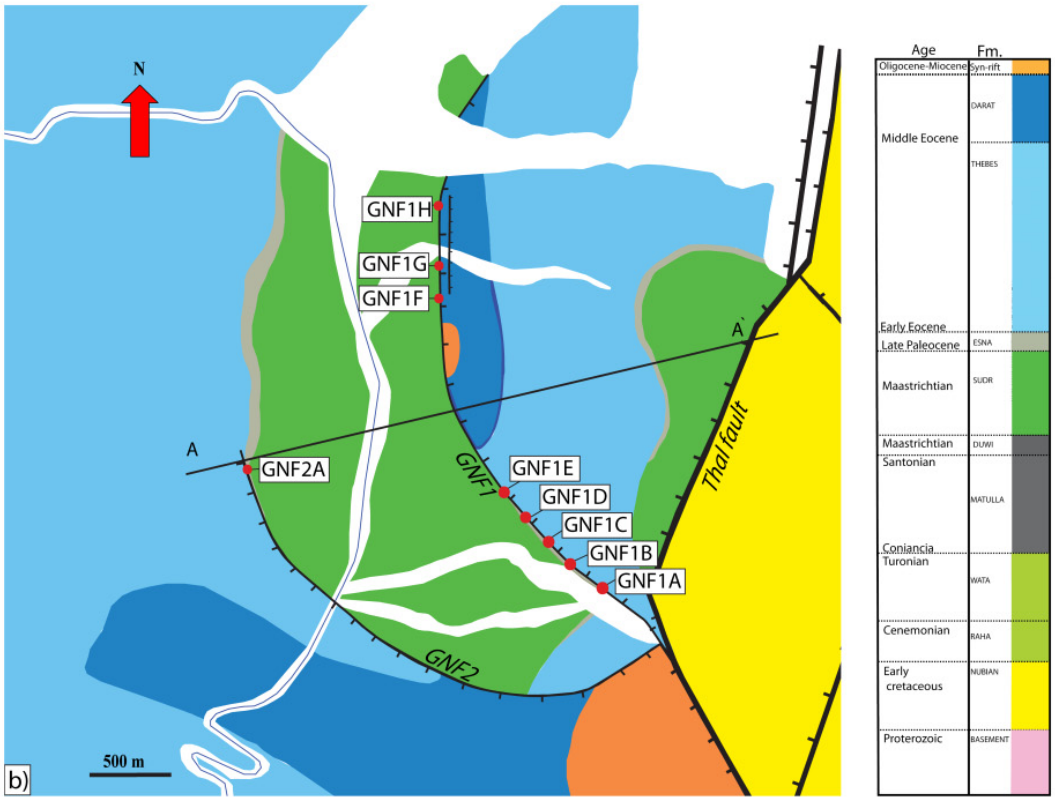

Fig 3.1: a) Satellite imagery over the study area, collected from Google Earth. b) Geological map of the study area, based on maps of Moustafa (2004) field mapping and satellite imagery from Google Earth. Next to the map is the stratigraphic column showing the different formations present. Line A-A` shows the location of the cross-section shown in figure 3.2. The localities for this study are marked with red dots and their associated names.

The Thal Fault (Fig. 3.1b) exhibits a throw ranging from 450 m up to 1200 m in the study area, with increasing throw values towards the south (Young et al., 2003).

The studied faults bound a horst, where the GNF1 is dipping mainly towards the NE-E, while the GNF2 is steeply dipping towards the S-SW (Fig. 3.2). GNF1 show dip values ranging from 45 -70 degrees with increasing dip values towards the north of the study area. While the strike of the fault is oriented NW-SE at the southern part of the area, the fault forms a bend and strike N-S in the northern part. GNF1 show increasing throw northwards. As shown on the geological map (Fig. 3.1b), GNF1 is segmented into smaller faults in the northern part of the area. GNF2 consist of a single segment and show decreasing throw values moving away from the Thal Fault. This fault tips out in the western part of the study area (Fig.3.1b), a locality which will be further described in chapter 3.4.1. Both of the studied faults links up with the Thal Fault in the south-eastern part of the area, and create a triple junction (Fig. 3.1b). The studied pre-rift formations in the area display a general westerly dip, except in the horst bounded by the two studied faults. While the strata in the horst dips to the west in the western part of the area, measurements show that the dip changes towards the south-eastern part, suggesting that the strata in the horst is folded into an anticline (Fig. 3.2).

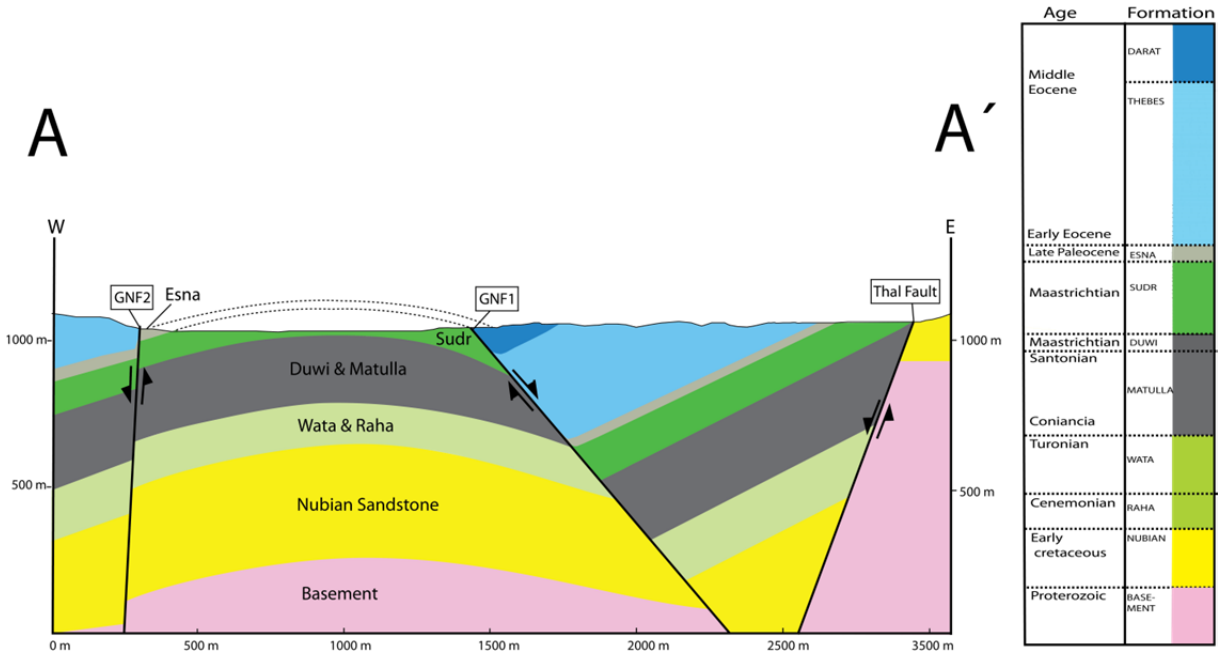

Fig. 3.2: Cross-section of the study area (location marked on figure 3.1b), based on maps of Moustafa (2004), field mapping and satellite imagery from Google Earth. The stratigraphic column to the right shows the associated name and ages of the different formations.

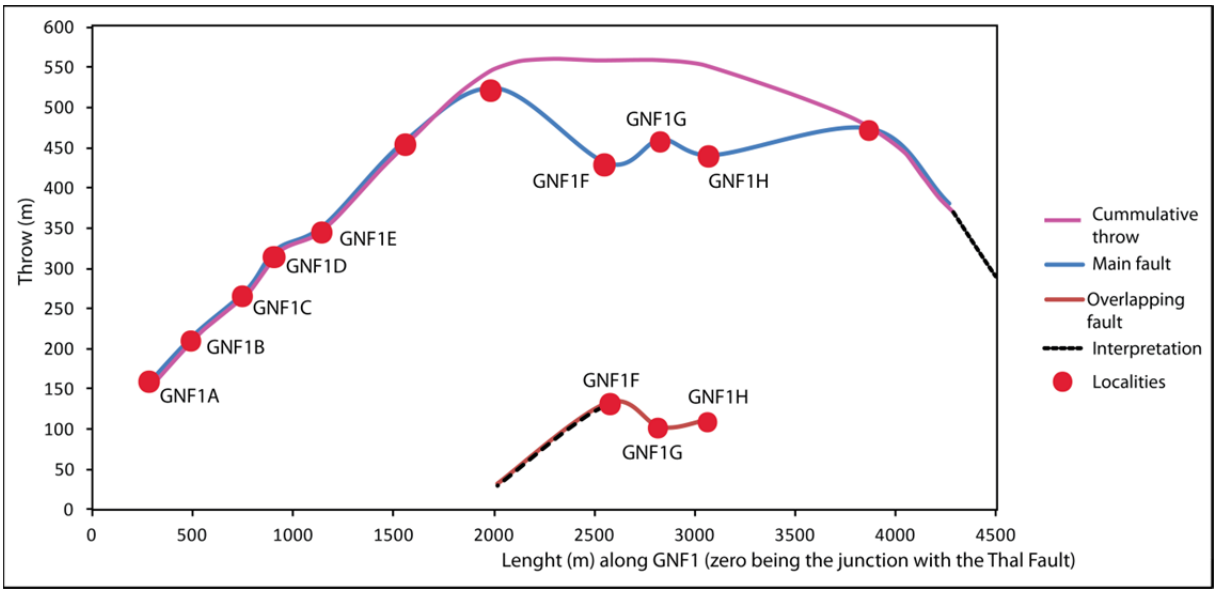

Fig. 3.3: Throw measurements from the different localities situated along GNF1, showing both the cumulative throw and the throw of the individual fault segments. The red dots correspond with the localities on the geological map (Fig. 3.1b). Some localities (unnamed red dots) have been chosen for throw measurements only and will not be included in the descriptions of the localities. The black dashed lines indicate interpretation.

Evidence of the anticline is also seen in the stratigraphy, where some of the upper part of the strata is repeated on both sides of the horst. The localities in this study are mainly located along GNF1, except locality GNF2A, which has been chosen due to the great opportunity to make observations in regard to early evolution of faulting (section 3.4.1). The throw measurements are therefore limited to GNF1, since observations in regard to throw only exist here. As shown in figure 3.3, the throw generally increase along the GNF1 towards the northern part of the study area. Close to locality GNF1F, two parallel faults are observed. This locality will be explained further in section 3.4.4.

3.3 Stratigraphy of the study area

The main rock units that have been studied are of Upper Cretaceous -Eocene age, which represent the middle part of the pre-rift period in the area. The exposed units consist of (from older to younger) the Sudr Formation, Esna Formation, Thebes Formation and the Darat Formation (Fig. 3.4). Two syn-rift basins are also present in the area (Fig. 3.1b), of which one of them (the southernmost) was mapped by Leppard & Gawthorpe (2006).

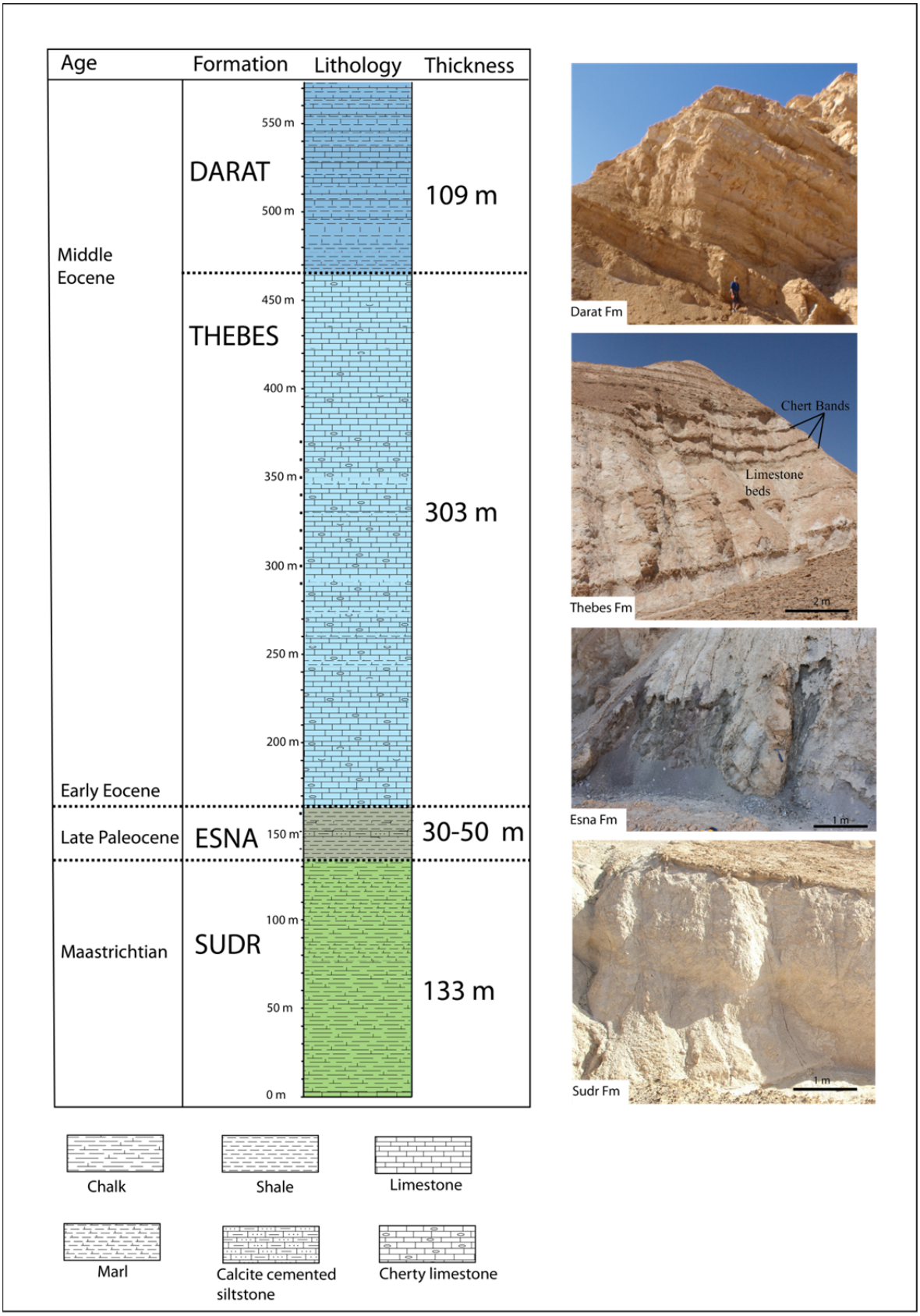

Fig 3.4: Lithostratigraphic column showing the studied pre-rift units and their representative ages. An example of each of the formations is added next to the column.

The second syn-rift basin is bordered by GNF1 (Fig. 3.1b) and was discovered during the current field study, and will (although outside the scope of this study) be described briefly in chapter 3.4.6. Present in the broader study area are also outcrops older pre-rift strata constituting the Matulla Formation, Nubian Sandstone and basement. Since these are not present in the successions affected by the studied faults, they will not be described in any detail here.

3.3.1 Sudr Formation

The Sudr Formation is the lowermost formation of the pre-rift carbonates exposed in the study area. Almost the entire Formation has been mapped (Fig. 3.4), except for the lowermost part which is not exposed. Thickness measurements in the area yield an estimated stratigraphic thickness of about 130 meters, yet exact estimates were difficult to obtain due to repetition of stratigraphy due to the anticlinal folding in the horst as described above. The lower and middle part of the formation consists of a massive, white, porous chalk. Moving up the succession to the upper part, the massive chalk becomes interbedded by a marly limestone. The thickness of the marly limestone beds and the chalk varies, both ranging from 1-5 meters. Hand specimens show high abundance of oysters and gastropods, especially in the lower part of the formation. Bioturbation is also observed in the area, especially in the lower part of the formation (Figure 3.5a). A sample from the chalk in the middle part of the formation was collected for thin section analysis (Figure 3.5b). The photomicrograph show high abundance of very fine biogenous material formed by 0.1-0.2 mm foraminifers, shell fragments and lime mud. The sample has been interpreted to be a grainstone after Dunhams (1962) classification scheme. To determine the content of the matrix surrounding the small shell fragments, SEM electron microscope was used. A photomicrograph (Fig. 3.5c) of the sample magnified 3.81 K, reveals that the matrix consists of coccolithophorid algae, which is calcareous nanofossils composed of calcareous plates (coccoliths) (Fig. 3.5c) (Boggs, 2001). Porosity is seen as micro porosity in the matrix (Fig. 3.5b) and as macro porosity represented by molds. The visible porosity is estimated to be around 10-15%, based on investigation of the photomicrograph. The permeability of the sample has not been tested, but assumed to be low due to high fraction of fine material and low connectivity between macro pores.

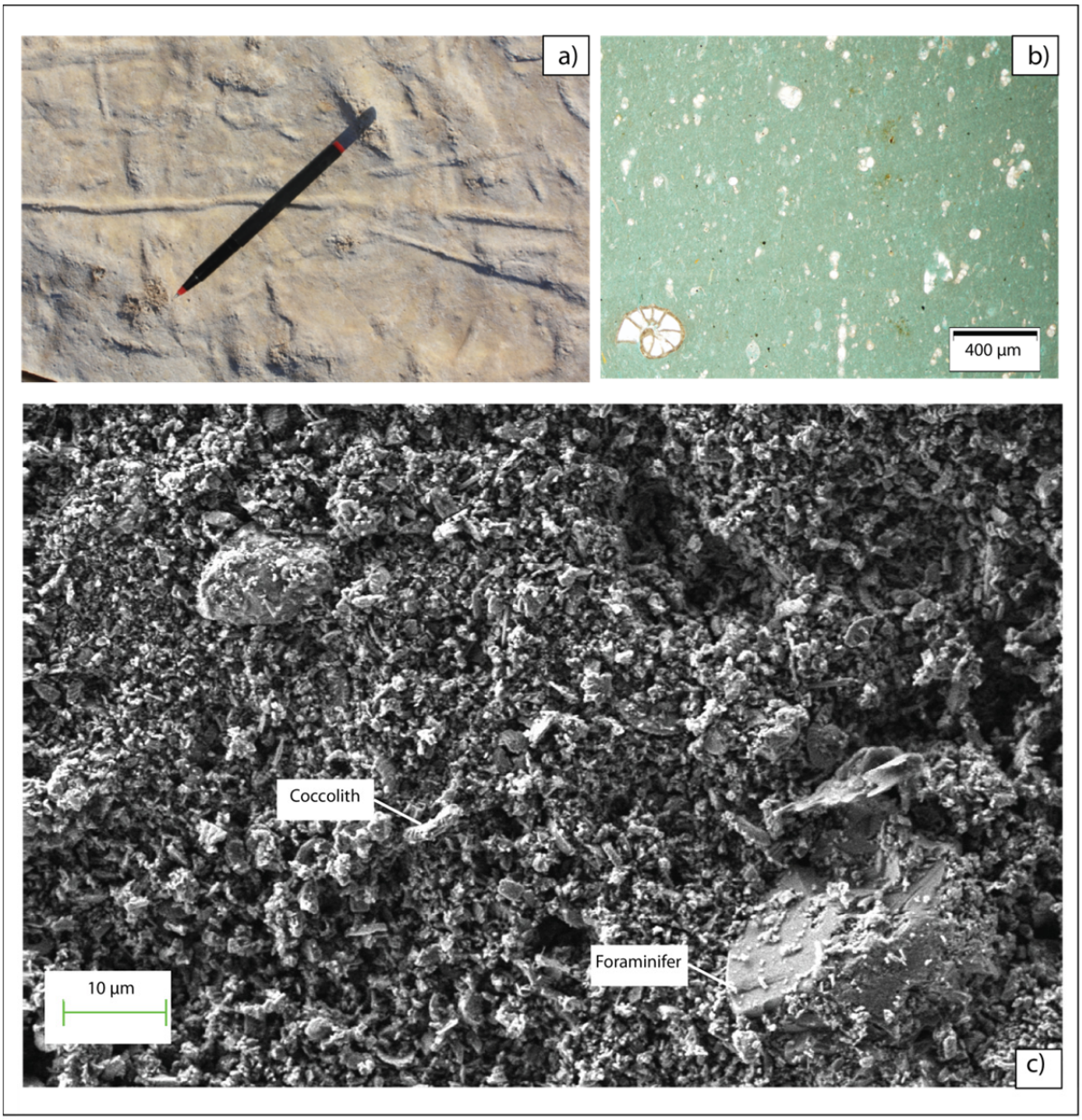

Fig 3.5: a) Bioturbation observed in the lower part of the Sudr Formation. b) Photomicrograph showing a sample from the chalk in the lower part of the Sudr Formation. The blue/green colour indicates porous material, which is dominantly in the matrix. Fossils are also observed in the sample, dominantly foraminiferas, and mainly coccoliths in the matrix. c) Photomicrograph using SEM electron microscope. The sample consists of predominantly coccoliths, but also some foraminifers.

3.3.2 Esna Formation

The Esna Formation (Fig. 3.4) has a greenish grey colour and is a good marker bed between the Sudr Formation and the Thebes Formation. The formation is shale, but two calcite cemented siltstone ledges are observed in the middle part, showing thicknesses of around 5 and 3 meters. In areas that are not affected by fault activity, thickness was measured to be approximately 50 meters, whereas close to the Thal Fault, the formation is rotated and has

likely experienced some layer parallel shearing, resulting in a thinning to approximately 33 m. In the shale smear analysis (section 3.4.5) the Esna shale thickness used is 50 meters.

3.3.3 Thebes Formation

The thickness of the Thebes Formation in the study area was measured to approximately 300 meters. The lower part of the formation is characterised by limestone beds interbedded with 10-20 cm thick chert bands. The middle part of the formation (Fig. 3.6a) consists of 2-4 meter thick beds of marly limestone, interbedded with meter thick limestone bed and thin chert bands (10-20 cm). The upper part of the formation is similar to the lower part, consisting of limestone beds interbedded with chert bands with some beds of marly limestone observed. The limestone beds have a thickness ranging from 20 cm to 1 meter. A sample was collected from one of the limestone beds in the middle part of the Thebes Formation. The photomicrograph (Fig. 3.6b) show high abundance of brown mud/clay, and a scarcity of bioclasts. This part of the formation has been interpreted as a mudstone after Dunhams (1962) classification scheme. The bioclasts observed are mainly gastropods and ostracodes along with some foraminiferas. The visible porosity is estimated to be between 0-2 percent based on thin section investigation, mainly seen as macro porosity represented by mould. The permeability is likely close to 0 in the sample, due to the high fraction of fine material and the fact that there is no visible connectivity between macro-pores.

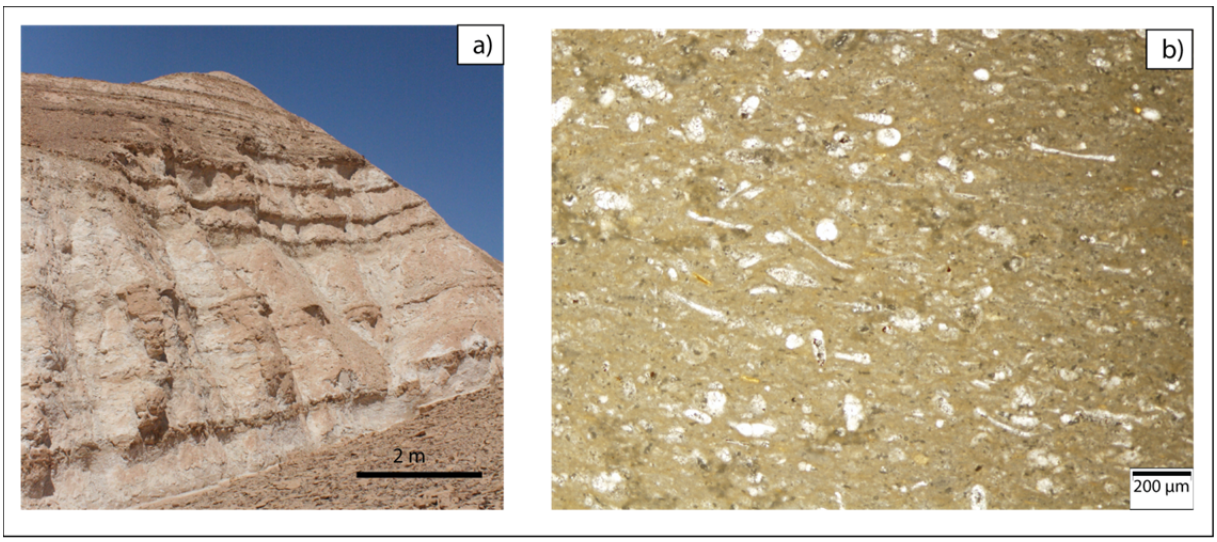

Fig 3.6 a) The figure displays the middle part of the Thebes Formation with limestone and interbedded chert b) Photomicrograph from one of the limestone beds in the middle part of the Thebes Formation. The sample consists of abundant clay with few fossils displayed, interpreted as a mudstone after Dunham (1962) classification scheme.

3.3.4 Darat Formation

The thickness of the Darat Formation was measured to approximately 110 meters in the study area. The lower part of the formation (D1) and the transition between Thebes Formation and Darat Formation is marked by a 20 m thick shale layer. A small bed of glauconitic sand is observed within this part of the formation, with abundant bioturbation (Bastesen and Rotevatn, in press). Limestone and marl beds are also seen in this part of the formation (Fig. 3.7a). The middle part of Darat (D2) features relatively thick limestone benches (2-4 meters), interbedded with thinner marl beds (0.5-1 meter). In the upper part of the formation (D3), the marl beds are thicker (2-4 meters), while the limestone beds are relatively thinner (0.5-1 meter). A sample has been collected from the limestone beds in the middle part of the formation. Thin section (Fig.3.7b) analysis show high abundance of bioclasts, and is interpreted as a grainstone after Dunhams (1962) classification scheme. The formation is made up of a wide range of fossils, i.e. gastropods, ostracodes, brachiopods, oysters and foraminifers. About 50% of the sample consists of bioclasts, surrounded by a porous matrix, which has been interpreted to be a mixture of lime and mud (Fig. 3.7b). The visible porosity is estimated to be around 10-15 %. Porosity is seen as micro porosity in the matrix and as macro porosity represented as mould. Due to the high fraction of fine material and low connectivity between macro pores, the permeability of the sample is assumed to be low.

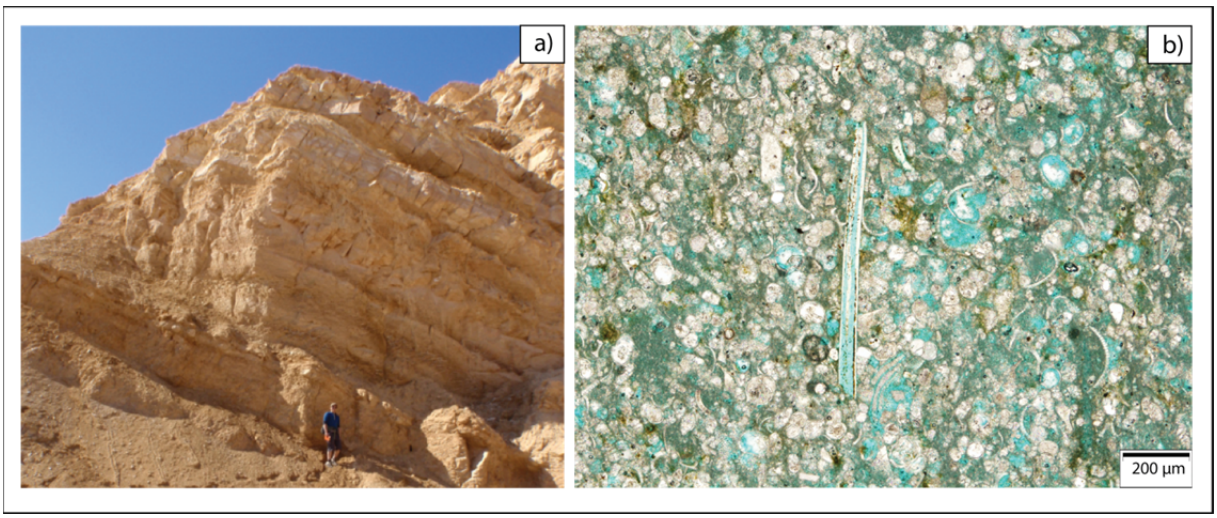

Fig. 3.7: a) The figure shows the transition between the lower and middle part of the Darat Formation. b) Photomicrograph of one of the limestone beds in the middle part of the Darat Formation (D2), reveals high abundance of fossils, surrounded by a porous, cryptocrystalline matrix.

3.4 Description of studied localities

The different localities chosen for this study are mainly located along GNF1 (Fig.3.1b) and displays successively increasing throw values moving northwards, ranging from 150 – 550 meters (Fig.3.3). One locality from the other fault, GNF2, was also included due to the great opportunity to make observations in regard to the tip-zone of the fault (Fig. 3.1b). The large variety of throw values along these faults, allow for a detailed study of the fault zone evolution. The localities will be presented from low to high throw values, hence describing the evolution of the fault zone and the associated changes in the fault core and inner damage zone. At low to intermediate throws (150- 320 m), shale gets entrained into the fault zone as smear, represented by locality GNF1A, GNF1B, GNF1C and GNF1D, situated at the south-eastern end of the GNF1 (Fig.3.1b). Locality GNF1D has been chosen as a key locality, representing fault zone with shale smear. At locality GNF1E, which also displays intermediate throw (350 m), the shale smear becomes discontinuous or absent: this is presented in section 3.4.3. Intermediate to high throws (350-550 m) is represented by locality GNF1F, GNF1G and GNF1H.

3.4.1 Tip zone of Gebel Nukhul Fault 2(GNF2): Fault propagation fold

Tip zones represent the front of propagating faults and thus provide opportunities to study the early stage evolution of faults. Locality GNF2A (Fig.3.8a) is situated near the lateral tip line of the GNF2, and is the last point where the fault is detected in the terrain. The throw has been recorded to be approximately 30 meters at this locality (total throw accommodated by folding and minor faults), juxtaposing the lower Thebes Formation with the Esna Formation. The Thebes Formation is dominated by faulting in the inner damage zone, with steep normal faults and with throw less than 10 meters. The formation at this locality is characterised by being folded into a monocline, which shows signs of being partly breached by faulting. The most steeply dipping limestone layers in the monocline are affected by low angle normal faults (5-15 degrees dip), with displacement of about 30 cm (Fig.3.8b and 3.8c). Since low angle normal faults like these are not mechanically feasible (Anderson, 1951), these faults have been interpreted to have been originally at a higher angle, and later rotated as a result of the formation of the monocline.

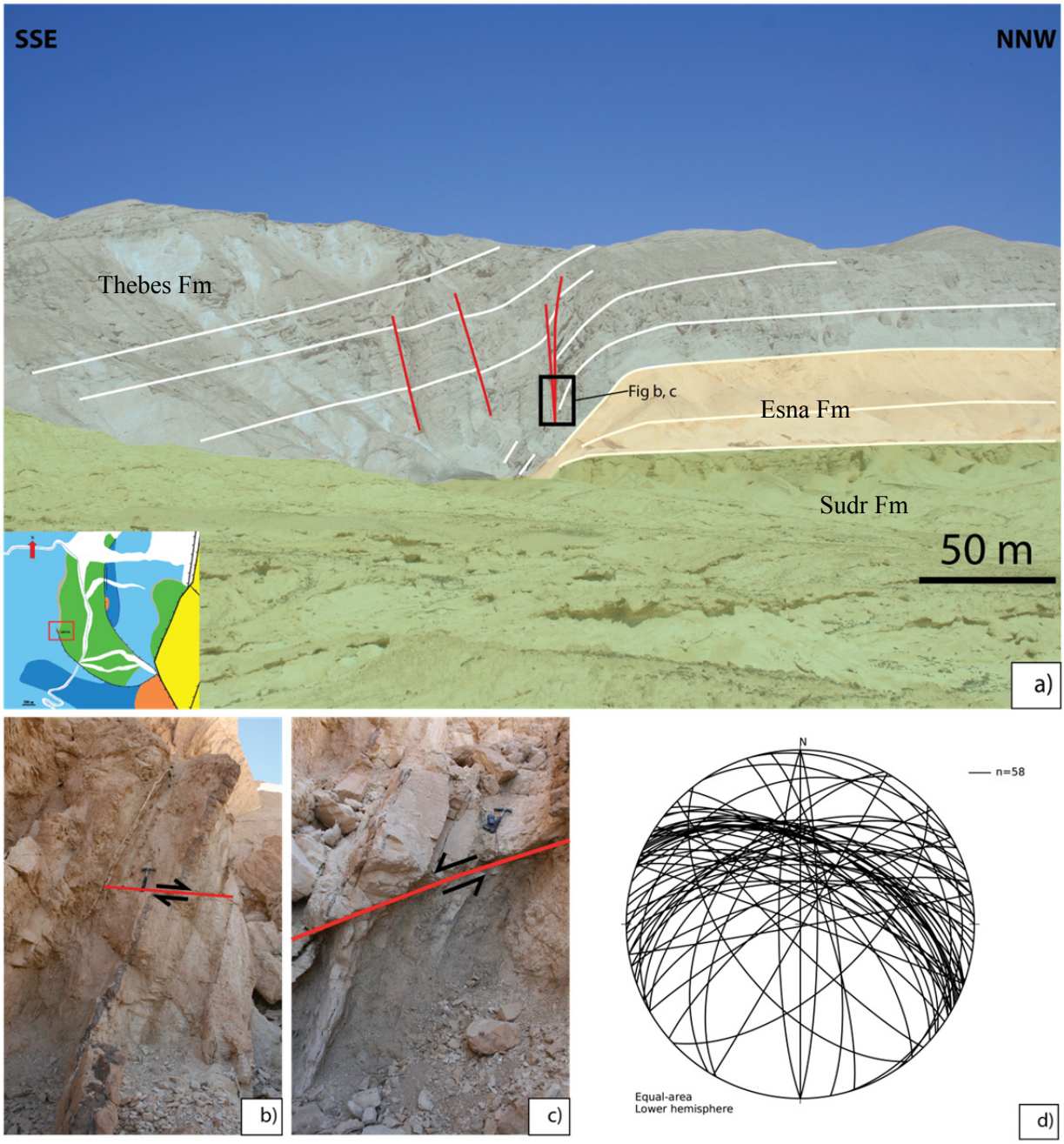

Fig 3.8: a) An overview of locality GNF2A, displaying a partly breached monocline, which represents a fault propagation fold. b) Limestone layers of the Thebes Formation, affected by low-angle normal faults (hammer for scale). These are interpreted to have been originally at a higher angle and later rotated to the present day low angle. c) same as b), d) Equal area, lower hemisphere stereonet of the fractures observed in the Thebes Formation, on the top of this locality where the fault is no longer detected in the terrain. The fractures show a NW-SE orientation, parallel with the fault plane.

Fracture measurements have been recorded on top of the monocline where the fault is no longer detected in the terrain. The fracture orientation measurements (Fig. 3.8d), show a high abundance of fractures oriented NW-SE, parallel to the main fault.

The partly breached monocline represents a fault propagation fold, a typical feature found near the tip-zone of a fault. The fault propagation fold and the resulting monocline are interpreted to have been formed by a combination of ductile and discrete brittle deformation. The fault propagation fold is affected by ductile deformation as reflected by the folding, but also by brittle deformation as reflected by the minor faults causing partial breaching of the fold.

3.4.2 Localities with shale smear along Gebel Nukhul Fault 1 (GNF1)

Four localities along GNF1 have been observed with shale smear derived from the Esna Formation. The localities are situated 300-1100 meters from the Thal Fault and its triple junction with the studied fault segments (Fig.3.1b). Three of the localities (GNF1A, GNF1B, and GNF1C) have extensive scree slope debris covering most of the fault core, and are therefore not suited for a fault core analysis. Due to the overall similarities of these three localities, they will be presented together. The last locality with shale smear (GNF1D) offers great exposure of both the fault core and inner damage zone and is therefore treated as one of the key localities representing the fault zone with incorporated shale smear.

3.4.2.1 Localities GNF1A, GNF1B, GNF1C

The localities displays increasing throw moving from GNF1A to GNF1C (Fig 3.3), offsetting successively more of the Thebes Formation, ranging from the lower part to the middle part. The footwall beds consist of the middle Sudr Formation, which are sub-horizontal at all three localities. The hanging wall fault block is affected by smaller scale (0.5 – 1 m throw) faulting near the slip-surface, and is at all the localities folded into a normal drag against the slip surface, dipping around 40 degrees to the NE with a strike parallel to the slip surface (Fig. 3.9). The extent of the normal drag is measured to be approximately 5 – 10 meters out in the inner damage zone of the hanging wall.

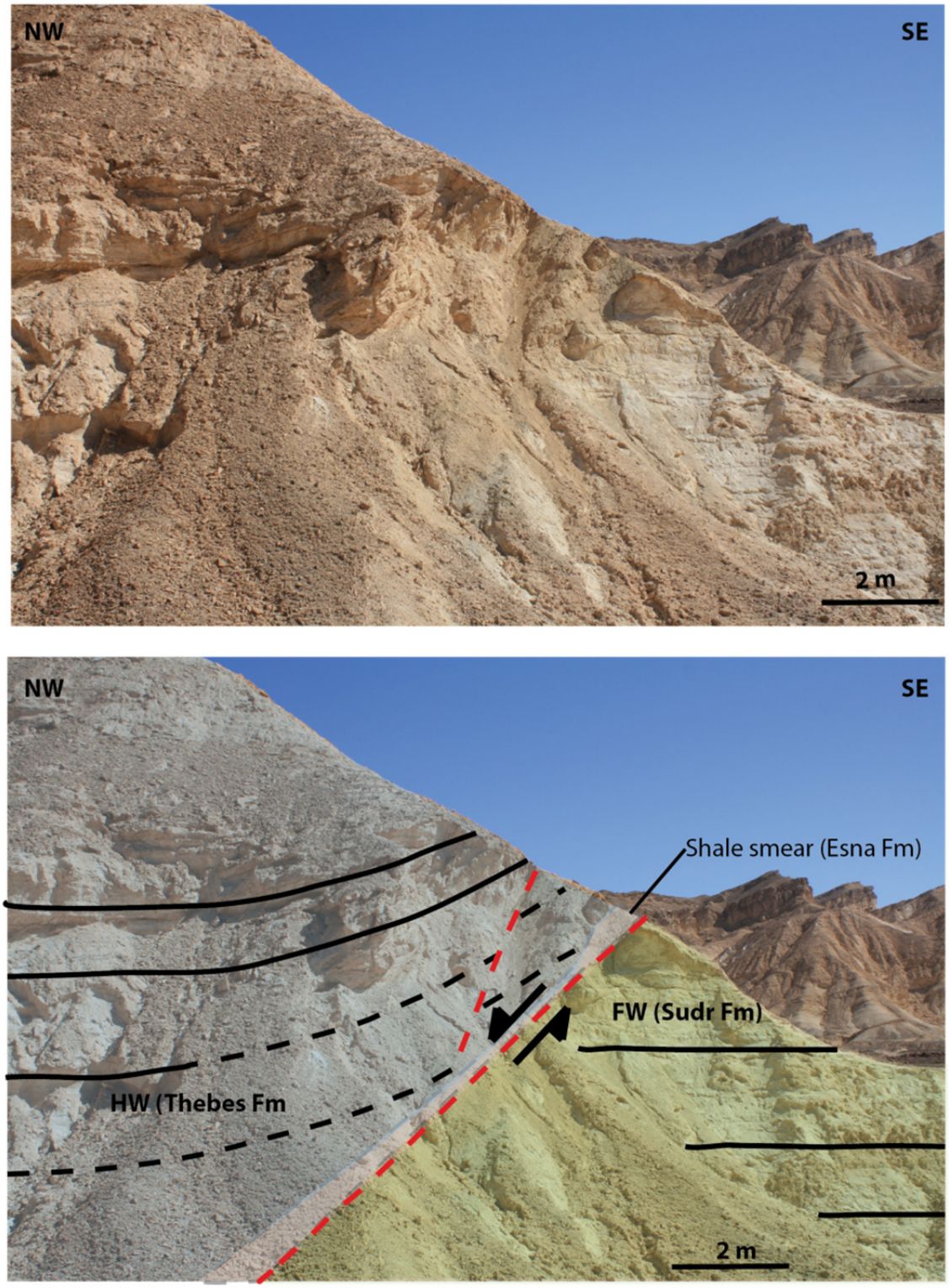

Fig 3.9: Due to the similarities of the three localities presented, they have all been summed up in this figure, displaying locality GNF1B. The fault core is represented by shale smear derived from the Esna Formation. As shown on the figure the Thebes Formation shows folding and small-scale faulting towards the slip surface.

Table 3.1: Key fault core data from GNF1A, GNF1B and GNF1C.

Locality	GPS (UTM)	Distance along fault (Measured from Thal Fault)	Throw	Altitude	Shale smear thickness	Orientation of slip surface
GNF1A	36R 522880 E 3213751 N	300 m	163	260	3-5 cm	298/45
GNF1B	36R 522733 E 3213918 N	630 m	213	273	5-50 cm	320/47
GNF1C	36R 522546 E 3214033 N	840 m	248	262	0,5 -1 m	319/47

Fault core

Table 3.1 summarises key data for the three localities presented in this section. Although the fault core was covered at most of the localities, some observations were made in terms of fault core composition. The fault cores consist predominantly of shale smear derived from the Esna Formation (Fig.3.9), ranging in thicknesses from only a few cm (GNF1A) up to 1 meter (GNF1C). One of the localities (GNF1A) also displays large calcite precipitations (5-10 cm thick) in the fault core, oriented parallel to the slip-surface. Only one prominent slip surface is exposed at each of the localities, striking NW with a dip value ranging from 45-47 degrees (Table 3.1). Due to the similarities of these three localities, the main trends in of the fault core and inner damage zone have been summed up in the figure displaying GNF1B (Fig.3.9).

Inner damage zone

The inner damage zone in the footwall is characterised by high fracture intensities, especially at GNF1A and GNF1B (Fig. 3.10). Fracture intensities in the footwall of the three localities are generally decreasing away from the fault core. The hanging wall is more stable, but tendency of decrease is also seen here (Fig. 3.10). Some fracture corridors, zones of significantly higher fracture intensities, are observed in both the footwall and hanging wall.

This is especially seen at locality GNF1B where the fracture intensity at 20 meters in the hanging wall increases from about 40 fractures per meter up to nearly 70 fractures per meter (Fig. 3.10). A wide range of fracture orientations is found in both the footwall and hanging wall, but two main trends can be detected. These are oriented sub-parallel and sub-perpendicular to the fault plane (Fig. 3.10).

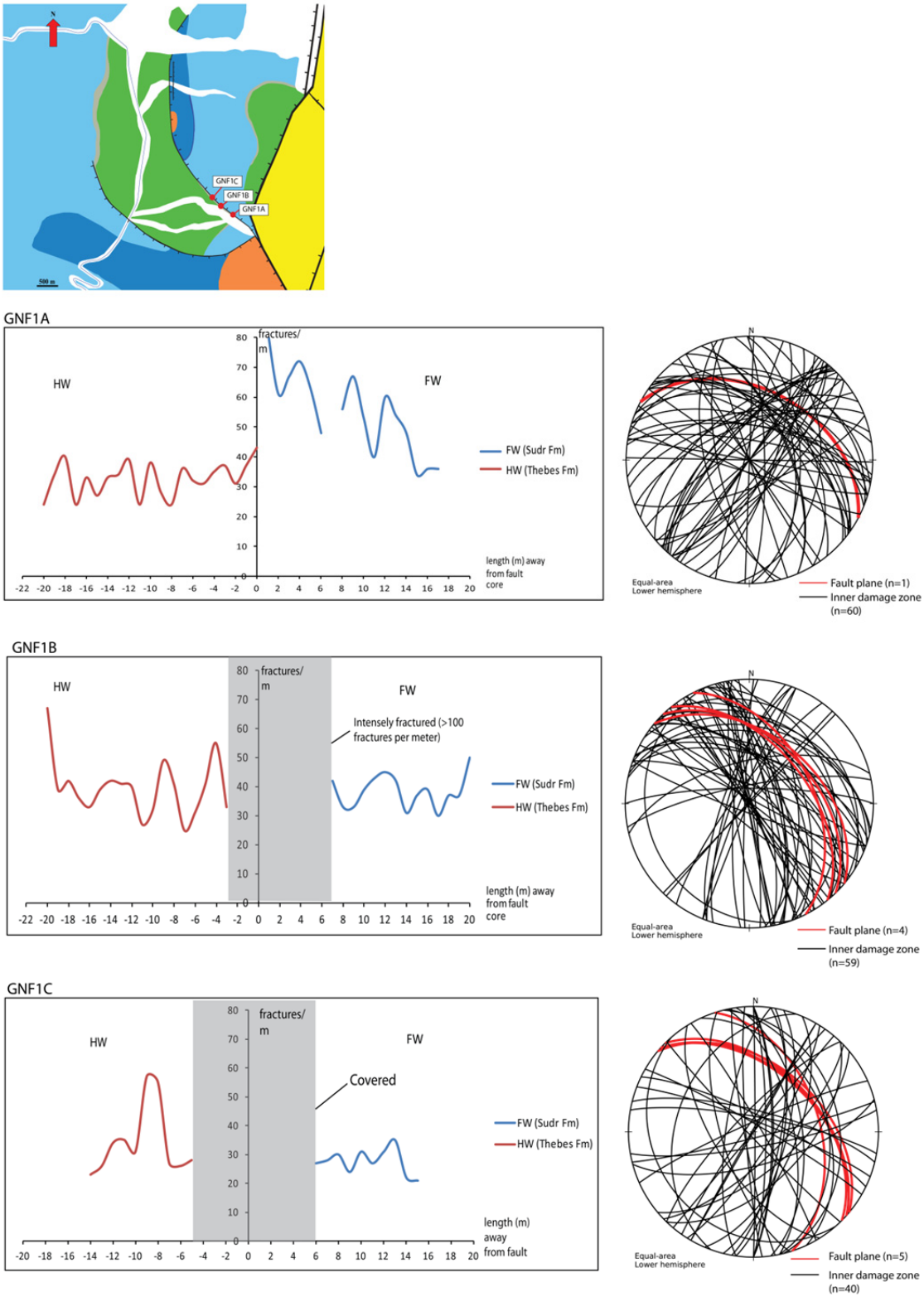

Fig 3.10: Fracture intensities observed at localities GNF1A, GNF1B and GNF1C, in both the hanging wall and footwall. Fracture orientations are shown as equal area lower hemisphere steronets, displaying both the fault plane and fractures in the inner damage zone. Fractures are mainly oriented sub-perpendicular and sub-parallel with the fault plane. Due to the high density of fractures at locality GNF1B, measurements were not possible, and are instead shown as a shaded area on the fracture intensity graph, indicating fracture intensities above a 100 fractures/meter. Due to extensive cover in the inner damage zone of locality GNF1C, fracture measurements were not collected here.

The fractures trending sub-parallel to the fault plane is dominated, especially in the footwall, by calcite cement with thicknesses between 2-30 mm. These fractures are long (m-scale), trough going and dominantly shear- and opening mode fractures. The fractures trending sub-perpendicular to the fault plane, are characterised as smaller in extent (5-20 cm), and exposed both as narrow unfilled fractures and small calcite cemented fractures.

3.4.2.2 Key Locality: GNF1D

The locality (Fig.3.11a) offers great exposures of both the fault core and inner damage zone, and is therefore treated as one of the key localities in this study, representing fault zone with incorporated shale smear. The locality is situated c.1100 meters from the Thal Fault and the triple junction (Fig. 3.11b). The hanging wall beds are comprised of the upper parts of the Thebes Formation, while the footwall consists of the middle Sudr Formation. The inner damage zone of the Thebes Formation is folded into a normal drag along the slip surface (Fig.3.11a), with fold limbs dipping up to 80 degrees NE, striking parallel with the fault plane. The extent of the normal drag is measured to be c. 30 meters out in the inner damage zone. The Sudr Formation is sub-horizontal at this locality (Fig.3.11a).

Fault core

The fault core displays three parallel primary slip surfaces (PSS). PSS-1 separates the Esna Formation and a fault rock lens derived from the Thebes Formation in the hanging wall, while PSS-2 separates the Esna Formation and a fault rock lens of the Sudr Formation in the footwall (Fig.3.11a). A third slip surface (PSS-3) is also seen separating the lens of the Thebes Formation in the hanging wall and the inner damage zone of the Thebes Formation (Fig. 3.11a). The overall orientation of the primary slip surfaces has been measured to be approximately 298/45 (Fig. 3.11e). Continuous shale smear derived from the Esna Formation is exposed (Fig.3.11a), with a thickness ranging from 5 cm up to 2 meters. Rock fragments of a calcite cemented siltstone are observed within the shale entrained along the fault, (Fig. 3.11c). The fragments are relatively large with a diameter up to 25 cm. These are interpreted to be derived from the limestone ledge that is observed in the middle part of the Esna Formation. The fault core also includes two fault rock lenses (Fig.3.11a), separated by shale smear derived from the Esna Formation. Both lenses are approximately 20 meters long, with a maximum thickness of c. 2 meters (Fig. 3.11a).

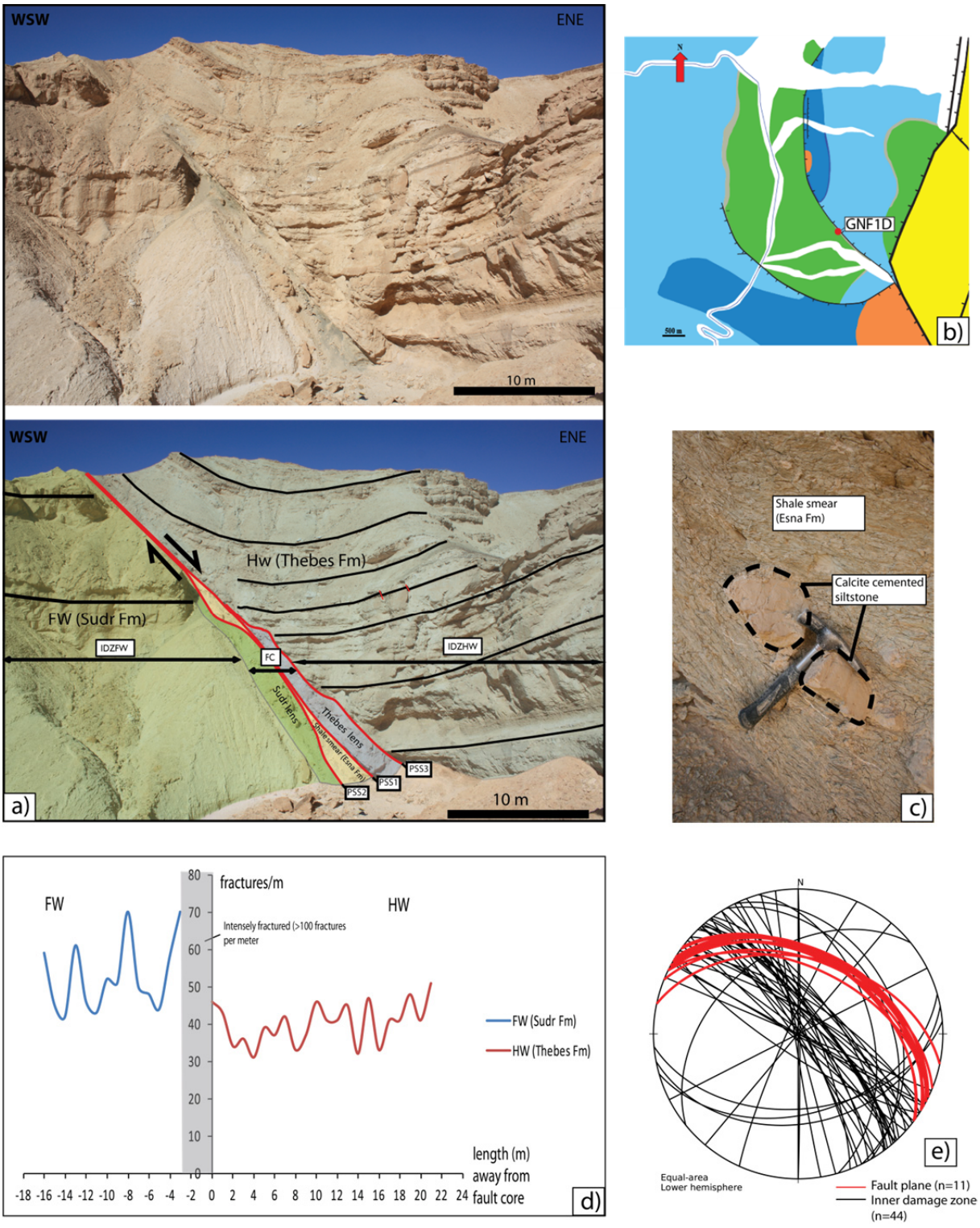

Fig 3.11: a) An overview of locality GNF1D the fault core where lenses of fault rock from the Sudr Formation and Thebes Formation are present along with shale smear derived from the Esna Formation. The Thebes Formation is steeply folded into a normal drag at this locality. (IDZFW-Inner damage zone footwall, IDZHW-Inner damage zone hanging wall, FC- fault core). b) Geological map showing the location of GNF1D. c) Rock fragments derived from the calcite cemented limestone ledge in the Esna Formation, situated in the fault core surrounded by shale. d) Fracture intensities for the inner damage zone both in the footwall and hanging wall. The grey area on the graph indicates fracture intensities >100 fractures/meter. e) Equal area, lower hemisphere stereonet of the fracture orientations both in the hanging wall and footwall, along with the orientations of the fault plane. The fractures are mainly oriented sub-parallel with the fault plane.

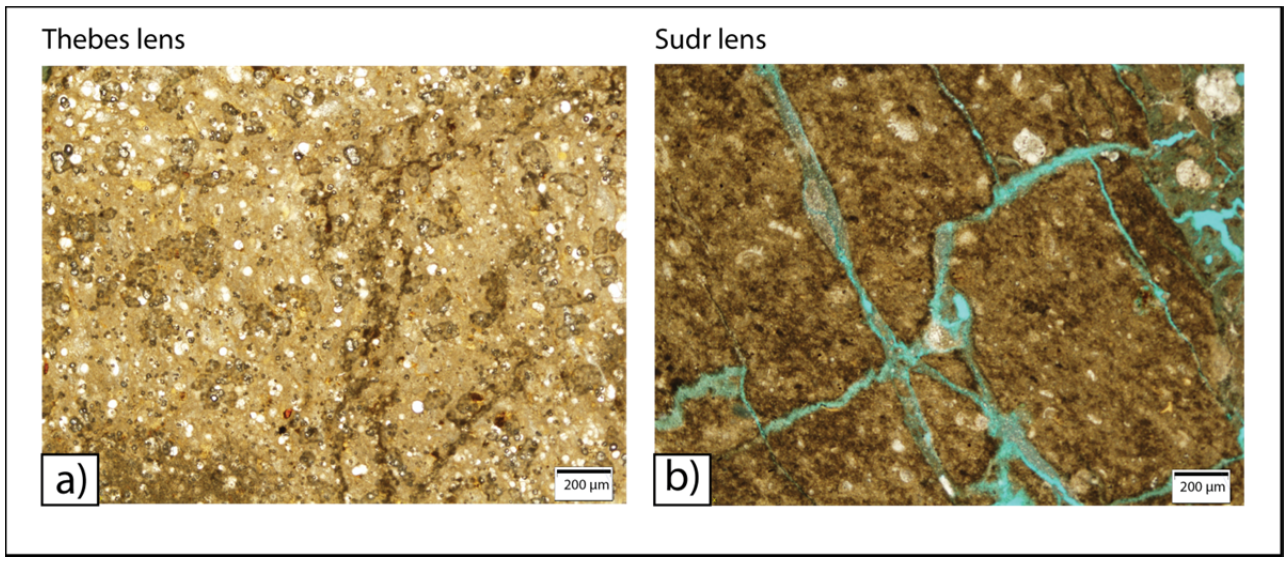

Fig 3.12: a) Photomicrograph of the fault rock lens derived from the Thebes Formation, interpreted as an indurated protobreccia. b) Photomicrograph of the fault rock lens derived from the Sudr Formation, interpreted as an indurated protobreccia.

The lens on the hanging wall side, derived from the Thebes Formation (Fig. 3.12a), display high clay content with some observed fossils, mainly foraminifers (0.2 - 0.3 mm). The sample consists of large clasts (c. 2 cm) which are mainly connected to each other. Between some of the clasts, a more porous matrix has been observed. The Thebes derived lens has been interpreted as an indurated proto breccia after Braathen et al. (2004) classification scheme. The lens on the footwall side, derived from the Sudr Formation (3.12b), consist of brown, clay rich clasts, surrounded by a more porous matrix. Due to the low fraction of matrix in the sample, this has also been interpreted as an indurated proto breccia. In the upper part of the fault rock lens derived from the Sudr Formation, abundant calcite precipitations are observed.

Inner damage zone

The inner part of the inner damage zone in the footwall consists of anastomising fracture sets. Although the fracture pattern here seems random, a higher proportion of fractures oriented similar to the strike of the fault plane is observed. The fractures in the innermost part of the inner damage zone are characterised by being small in extent (5-20 cm) and comprising both narrow calcite cemented fractures and unfilled fractures. The footwall displays a higher fracture intensity compared to that of the hanging wall (Fig. 3.11d). While the footwall shows a decrease in the fracture intensity moving away from the fault core, the hanging wall show much more stable fracture intensities. Especially in the footwall, several fracture corridors are

observed with intensities up to 70 fractures per meter (Fig.3.11d). The fracture corridors are characterised by more anastomisong fracture patterns, with some long, through going, calcite filled, fractures oriented parallel with the fault plane. The fractures at the locality are mainly opening mode and shear fractures. The dominating orientation is sub parallel-parallel with the fault plane and sub-perpendicular (Fig. 3.11e). Red, irregular seams are observed striking perpendicular to the main direction of fractures and the fault plane. These have been interpreted as pressure solution seams.

3.4.3 Locality without shale smear along Gebel Nukhul Fault 1 (GNF1)

3.4.3.1 Key locality without shale smear: GNF1E

The locality is situated about 1300 meters from the triple junction and the Thal Fault (Fig. 3.1b). The fault succession is comprised of beds of the upper Thebes Formation in the hanging wall and the beds of the middle Sudr Formation in the footwall. Also this locality has great exposure of both the fault core and inner damage zone. The locality is a key locality representing fault zone without continuous shale smear. The Thebes Formation is also folded into a normal drag at this locality (Fig.3.13a), but with less steep fold limbs than the previous locality (35 degrees dip) and only extending 5-10 meters out in the hanging wall. Minor faulting in the hanging wall close to the slip surface is observed with relatively small displacement (>0, 5 m). The layers of the Sudr Formation show sub horizontal dip.

Fault core

The fault core is bounded by two parallel primary slip surfaces (PSS). The slip surfaces, which are located 2.4 m from each other, have an orientation of 309/52. PSS-1 is more prominent and a thin, discontinuous clay membrane, which may be remnants of the Esna Formation, is observed along this slip surface, bordering the inner damage zone of the Thebes Formation (Fig.3.13a). Also precipitations of calcite are observed along PSS-1. PSS-2 separates the fault core and the inner damage zone of the Sudr Formation (footwall). The fault core comprises several fault rock lenses, derived from Sudr Formation. The different lenses have been divided into three different domains, based on observations in field (Fig. 3.14a). The lenses are separated by a thin (mm-scale) clay membrane.

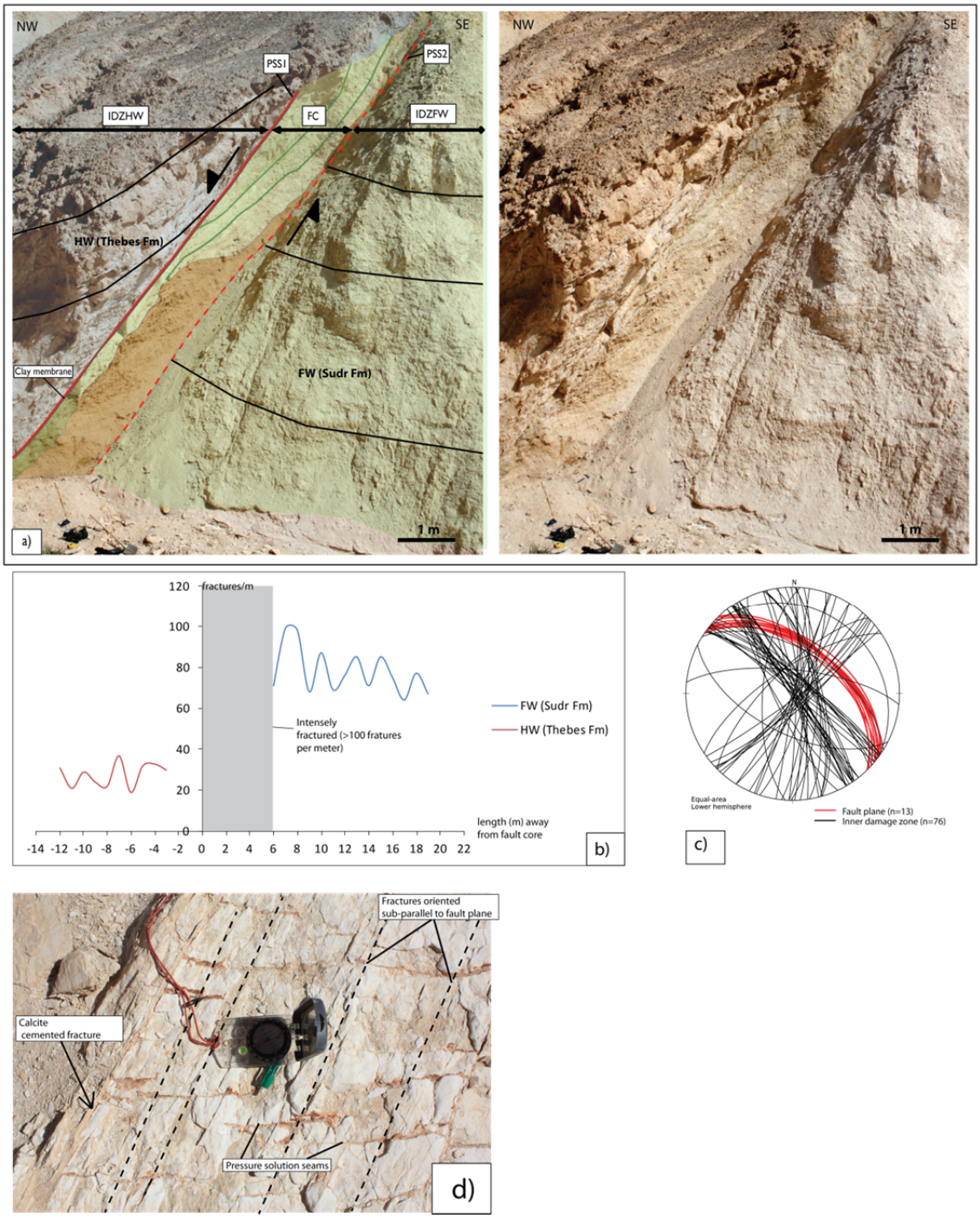

Fig 3.13: a) An overview of locality GNF1E showing both the fault core and inner damage zone of the locality. For location of GNF1E, see figure 3.1b. (IDZH-Inner damage zone hanging wall, IDZFW- Inner damage zone footwall, FC- fault core) The composition of the fault core is explained in figure 3.14. b) Fracture intensities of the inner damage zone in both the footwall and hanging wall. The grey area on the graph indicates intensely fractured areas with intensities of 100+. c) Equal area lower hemisphere stereonets displaying the orientations of fractures in the inner damage zone (black) and the fault plane (red). The fractures are oriented mainly sub-parallel and sub-perpendicular to the fault plane. d) Pressure solution seams observed in the footwall, oriented perpendicular to the main fracture direction. These are interpreted to be pressure solution seams.

A hand specimen from Domain 1 (Fig.3.14), reveals relatively large, white, clasts (up to 1 cm), mainly connected with each other, surrounded by a grey matrix. Areas with smaller, white clasts (1-2 mm) surrounded by grey matrix are also observed, but to a lesser extent. Photomicrographs (Fig. 3.14) from this domain display high clay content both in the clasts and the surrounding matrix. The clasts have a light brown colour, while the surrounding matrix shows a darker brown colour. Both the clasts and the matrix contain fossils. (Fig. 3.14).The samples are dominated by angular clasts, but some rounded clasts are also observed.

Hand specimen from Domain 2, is mainly dominated by smaller clast sizes (0.5-1 mm) compared to Domain 1, but also some larger clasts are also observed (c. 1cm). The white clasts are both angular and rounded, surrounded by a grey, clay rich matrix (Fig.3.14). The thin section displays similar features as in Domain 1, where light brown clasts are surrounded by a darker brown matrix, suggesting high clay content. Several of the fossils are connected to each other and show pressure solutions seams in the grain contact. Using a SEM electron microscope, the main elements of Domain 1 and 2 was revealed. The domains are dominated by NaCl and Ca.

Domain 3 is situated below the exposed lenses, and consists of a brown, soft material, with high abundance of calcite and gypsum precipitations. This part of the fault core has been interpreted as a marl-bed from the Sudr Formation. The thin section reveals high abundance of clay, but with some areas showing some micro porosity. The observations and classification of the lenses will be discussed in chapter 5.

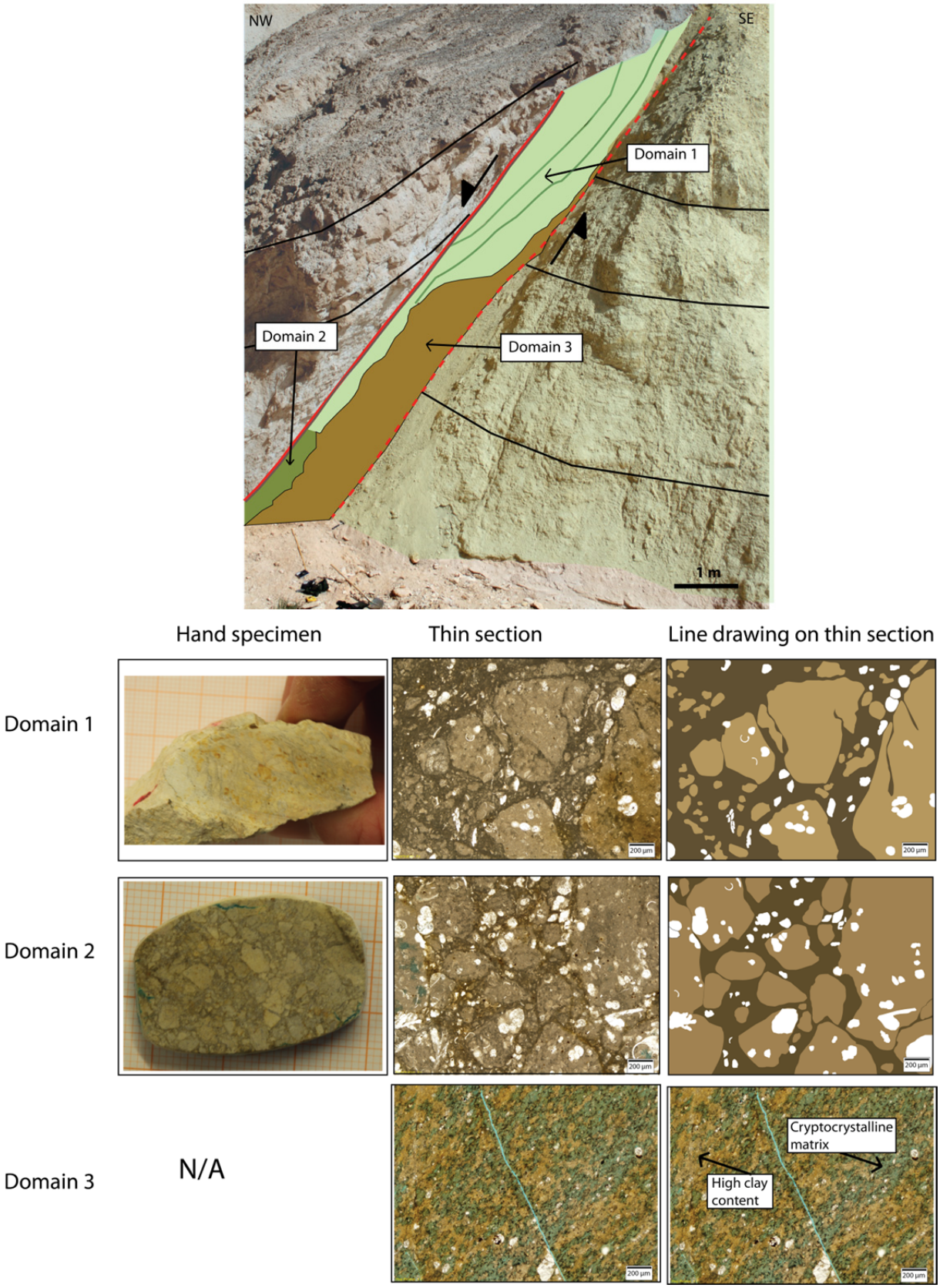

Fig 3.14: The fault core has been divided into three different domains. Hand specimen and photo micrograph is shown for each of the domains (except domain 3). Domain 1 and 2 show similar features, especially in the thin section, where light brown clasts of clay is surrounded by a darker brown matrix, also containing clay. The clasts are mainly observed to be angular. Underlying domain 1 and 2 is a thick bed of a marly limestone, which shows abundant clay with some areas of increased porosity.

Inner damage zone

The innermost part of the inner damage zone in the footwall is characterized by intensely fractured rocks, showing anastomising fracture patterns. Although the orientations seem random, orientations sub-parallel to the fault plane are more abundant. This part of the damage zone is shown as a shaded area on the fracture intensity graph (Fig.3.13b), showing fracture intensities of over 100 fractures per meter. Due to cover in the innermost meters of the hanging wall, no fracture measurements were collected here (Fig. 3.13b). The fracture intensity seems to be higher in the footwall compared to the hanging wall (Fig.3.13b). Especially in the footwall, a decrease in fractures per meter is shown moving away from the fault core. The fractures are oriented mainly parallel-sub parallel with the fault plane (Fig.3.13c). The fractures in the footwall are observed to consist of 1 – 30 mm thick calcite precipitations, ranging up to several meters in length. The fractures both in the hanging wall and footwall are mainly opening mode and shear fractures. Fractures trending sub-perpendicular to the fault plane are also observed (Fig. 3.13c), but with smaller extent (5-20 cm long), both narrow unfilled fractures and calcite cemented fractures. Also at this locality, red, irregular seams are observed, oriented sub-perpendicular to the main fracture orientation and fault plane (Fig.3.13d). These are interpreted to be related to pressure solution, and may therefore represent pressure solution seams.

3.4.4 Fault overlap zone (Locality GNF1F, GNF1G, GNF1H)

In the northern part of the study area, the main fault becomes overlapped by a second fault, showing the same trends in orientation, striking N-S and dipping to the east. The two fault segments bound a fault overlap zone (relay zone), which is shown in figure 3.15, a close up of this part of the study area. As a result of changes in the throw (Fig.3.3), the segment alternates between the Thebes Formation and the Darat Formation (Fig.3.15). As shown on the throw plot for these faults, the throw values show several throw minima, which will be discussed further in chapter 5. Several characteristic changes in the fault core and inner damage zone have been observed in this part of the study area and will be described in the next section.

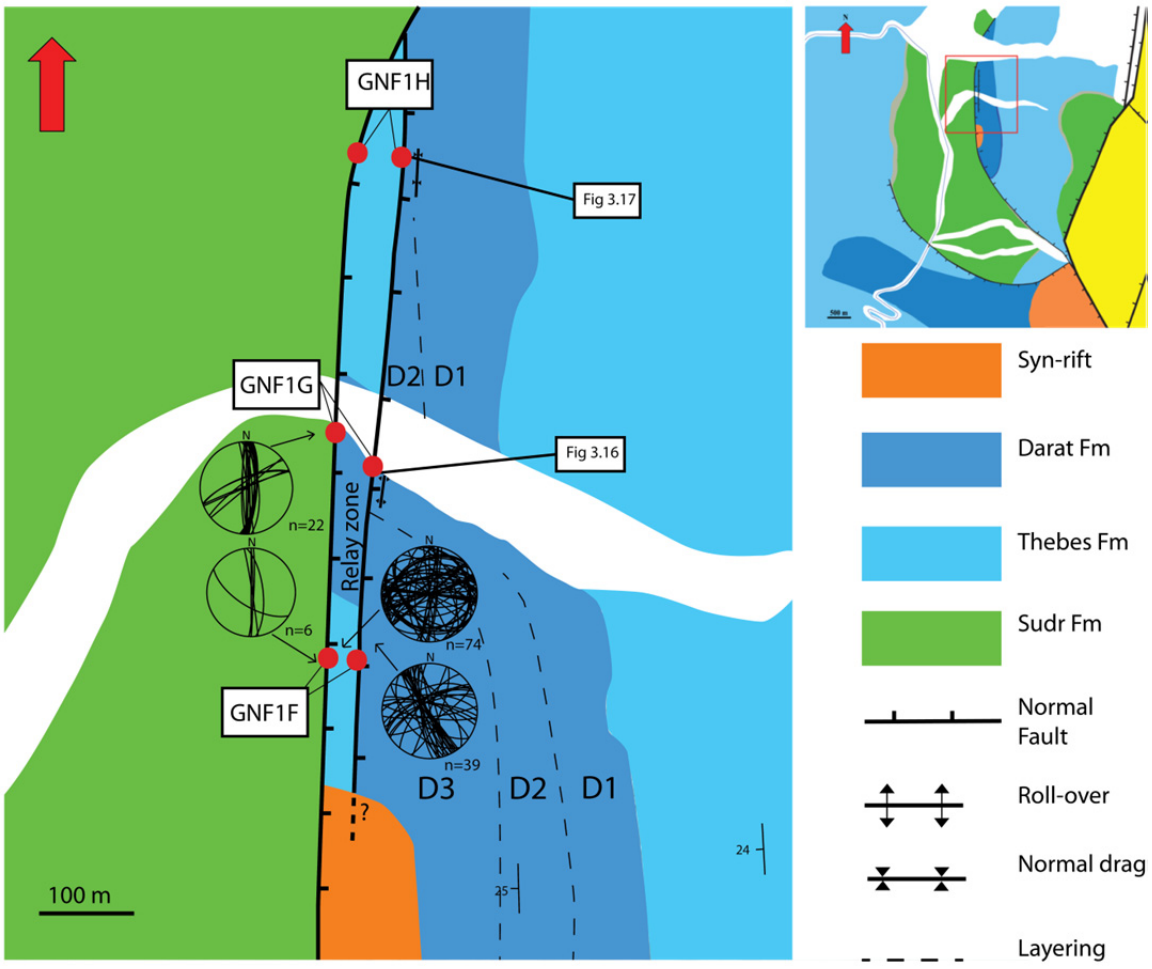

Fig 3.15: Northern part of the study area where two overlapping faults are observed, bounding a relay zone. The figure displays the locations of GNF1F, GNF1G and GNF1H. Fracture orientations have been measured at some of the localities, represented with equal area lower hemisphere stereonets and arrows for the location of the measurements. D1, D2 and D3 represent the different parts of the Darat Formation (chapter 3.3.4). The second segment is not detected south of locality GNF1F and is therefore only shown as a dashed line. The figure also displays the location of figure 3.16 and 3.17. Hanging wall folding is also indicated on the map, where locality GNF1G display a rollover structure, while GNF1H display normal drag.

Fault core

The fault core of the western most fault show the same characteristics extending northwards through this part of the study area. The fault core consists of a slip surface, high abundance of calcite precipitations and some clay. The thickness of the fault core has been measured to be around 10-20 cm at the different localities. The slip surface has an orientation of approximately 005/70.

The fault core of the eastern fault segment displays quite a different character, both in composition and thickness. The fault core has been studied at three different localities, and shows a change in thickness and character moving from south to north. At the locality GNF1F (Fig.3.15), where the Thebes Formation has been observed in the relay zone, juxtaposing the

upper part of the Darat Formation (D3), a small lens, interpreted to have been derived from the lower part of the Darat Formation (D1) is displayed in the fault core, with a thickness of about 1.5 meters. Further north (250 m), at locality GNF1G, the composition and orientation of the fault plane changes (Fig.3.16). The overlapping fault juxtaposition the middle Darat Formation (D2) and the lower Darat Formation (D1), and creates a listric shape of the fault plane (Fig.3.16), changing in dip from c. 60 degrees at the top, down to c. 40 degrees at the base. The fault core consists of shale smear derived from the lower part of the Darat Formation (D1), displaying high abundance of clay and fragments of marly limestone. The layers of the inner damage zone of the hanging wall (D2) are dipping down towards the fault plane, creating a small anticline structure (Fig. 3.16). The anticline structure only affects the innermost 5-10 meters of the hanging wall. High abundance of small scale normal faulting (> 0.5 meters) is also observed at the locality (Fig.3.16).

Towards locality GNF1H, the throw of the eastern fault segment increases (Fig 3.3), and a large scale lens (thicknesses up to 15-20 meters) is observed in the fault core (Fig. 3.17). This is interpreted to be derived from the lower part of the Darat Formation (D1). The lens show high abundance of clay, along with some marl. A thin bed of glauconitic sand is also observed in the fault core, also suggesting that the lens is derived from the lower part of the Darat Formation (D1) (section 3.3.4).

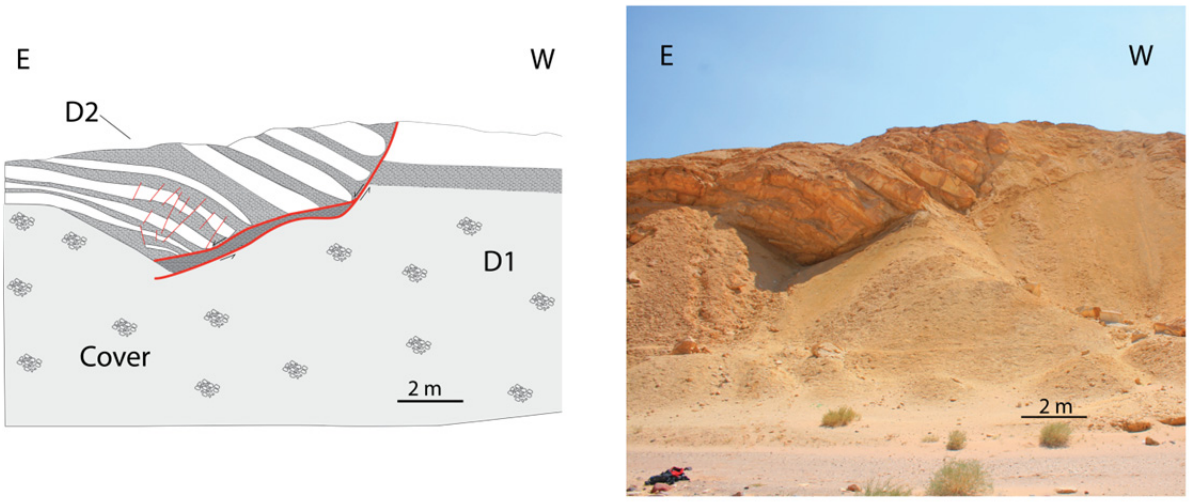

Fig 3.16: The figure shows the small anticlinal structure which is associated the easternmost fault at locality GNF1G. While the white layers indicate limestone beds, the grey layers indicate marl and shale. As seen from the figure, a small lens of shale smear derived from the lower part of the Darat Formation is exposed in the fault core. Pronounced faulting in the hanging wall of the Darat Formation is also observed, indicated with red lines.

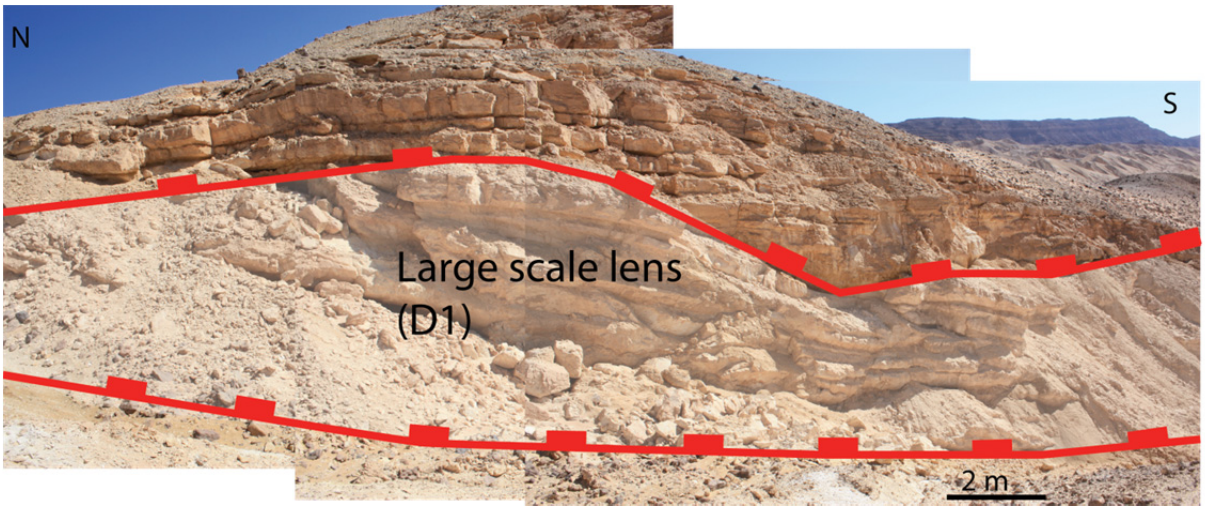

Fig 3.17: Large scale lens at locality GNF1H observed at the easternmost fault, close to where only one fault is observed (Fig.3.15). The lens consists of predominantly shale derived from the lower Darat Formation (D1), exposed with some marl and limestone.

Fracture patterns in the relay zone

The inner damage zone of the faults in this area is characterised by being covered and inaccessible, but a few localities allowed for fracture measurements to be carried out. At locality GNF1G, in the footwall (Sudr Formation) of the westernmost fault segment, fracture measurements revealed an average of 30 fractures per meter in the innermost 10 meters of the inner damage zone. No distinct difference in the fracture intensity was observed moving towards the fault plane. The fractures are mainly oriented sub-parallel to the fault plane (Fig.3.15) with both calcite cemented and narrow unfilled fractures. The thickness of the fractures has been measure to be around 5-10 mm.

At locality GNF1F, fracture measurements were collected in the fault bounded segment where the Thebes Formation is exposed (Fig. 3.15). The orientations of the fractures (Fig.3.15) show no clear trend, displaying orientations in all directions. The fractures are mainly calcite cemented with thicknesses up to 25 mm. Fracture intensities measurements from the Thebes Formation show relatively higher fracture intensities than what has been observed at the previous localities, with an average intensity around 60 fractures per meter in the fault bounded segment. Fracture orientations of the Darat Formation (Locality GNF1F), which is exposed in the hanging wall of the easternmost fault segment show orientations mainly sub-parallel with the fault, but also sub-perpendicular (Fig.3.16).

3.4.5 Shale Smear Factor

Based on the throw of GNF1(Fig. 3.3) and the thickness of the source layer, which in this context is the Esna Formation, displaying a thickness of approximately 50 meters, the shale smear factor (SSF) have been calculated for all of the localities which have been studied (Fig. 3.18). Shale smear factors have only been calculated for the GNF1, since this is mainly where the localities are situated. In the shale smear factor calculations, cumulative throw values have been used (Fig. 3.3). The calculated shale smear factor for this fault shows that shale smear appears continuous for a shale smear factor up to 6.5, and that the shale smear becomes discontinuous for shale smear factors over this number. The calculated shale smear factor will be compared and discussed with other studies on this subject in the discussion (chapter 5).

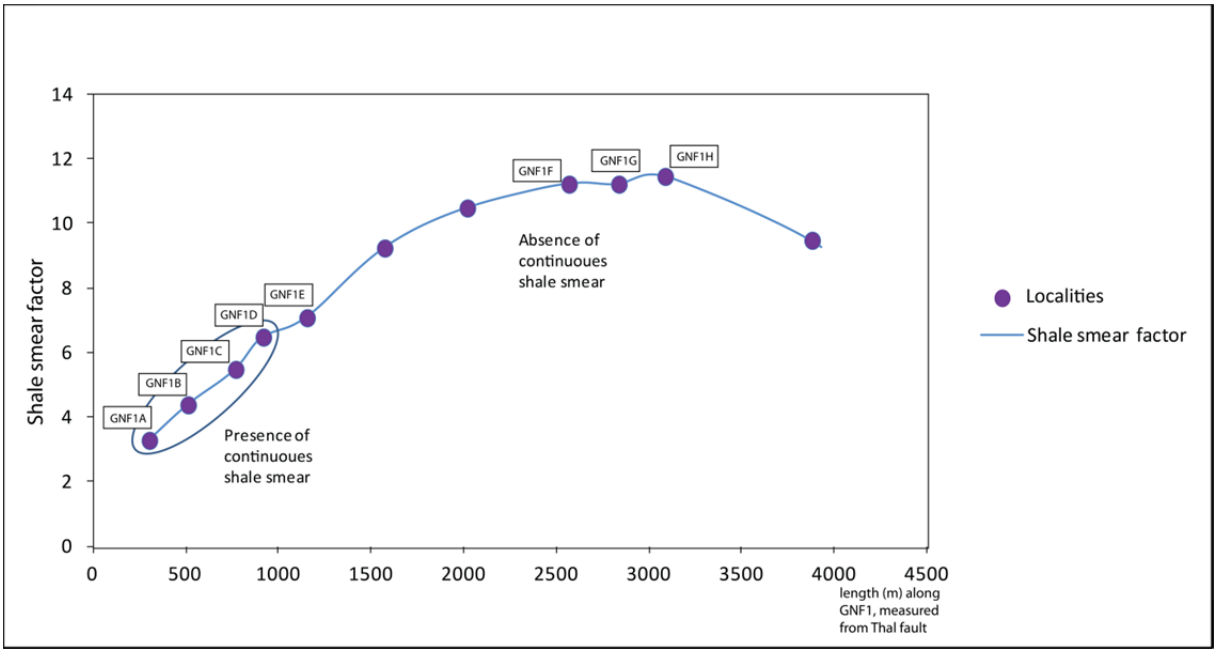

Fig. 3.18: The calculated shale smear factor for GNF1, displayed as a function of distance along the fault. All the studied localities are marked on with their names (see figure 3.1b for location). The localities with continuous shale smear are circled, while the rest of the localities display no continuous shale smear (from the Esna Formation). The shale smear factor is calculated by dividing the throw of the fault on the thickness of the source layer (Lindsay et al., 1993).

3.4.6 Syn-rift basin

Close to the throw maximum of the GNF1, a small syn-rift basin (Fig. 3.19) is located, extending about 3000 m^2. The sediments in the basin are unconformably overlying the Darat Formation, displaying a different dip angle than the rest of the pre-rift rocks. The syn-rift strata show some degree of thickening towards the GNF1 (Fig.3.19), where the layers are seen to fold slightly towards the fault, suggesting deposition while the fault was still active. The lower part of the sediment package are observed to consist of red, medium coarse deposits, interpreted to be part of the Abu Zenima Formation (Fig.3.19). The thickness of the Abu Zenima Formation is measured to be between 0.5-1 m. Overlying the Abu Zenima Formation is a unit dominated by coarse grained clasts, surrounded by finer grained material. The package is coarsening upwards and show signs of being crossbedded. These are interpreted to be part of the Nukhul Formation (Fig.3.19). The formation is observed to be thicker than the Abu Zenima Formation, between 5-10 meters.

The mapping of the syn-rift basin has been done primarily to be able to indicate an age relation on the studied faults. The evolution of the studied faults and their relationship to the Thal fault will be discussed more in chapter 5.

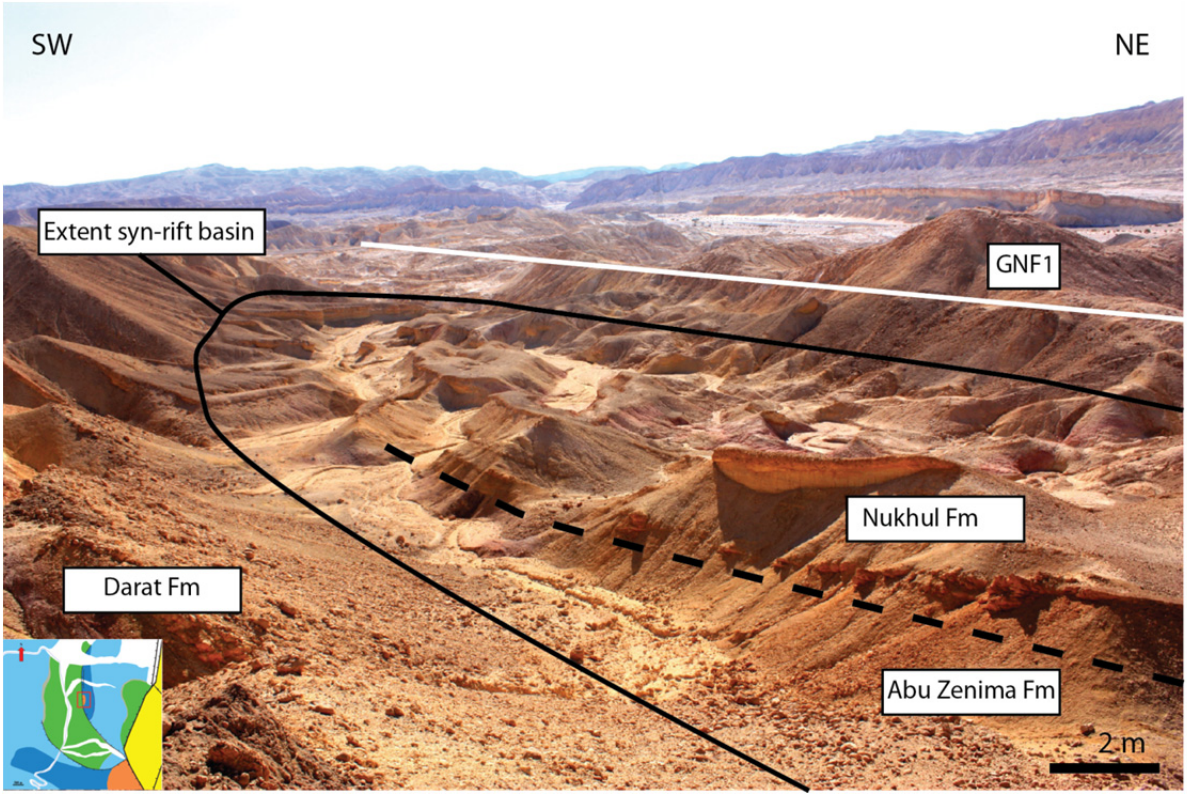

Fig. 3.19: The figure displays the small syn-rift basin which is located close to the throw maxima of GNF1. The trace of GNF1 is shown as a white line. The formations present in the basin are interpreted to be the Abu Zenima Formation and the Nukhul Formation. The syn-rift strata show some degree of thickening towards the GNF1. Folding of the layers towards GNF1 is also observed.

4. Statistical analysis of data

Part of the aims of this study is to discuss whether there is a significant difference between fault zones with entrained shale smear and fault zones where the shale smear is absent. In order to assess whether or not there is a significant difference between the fracture populations, statistical analysis of the fracture intensities have been carried out. As presented in the previous chapter, fracture intensities have been collected at the different localities. In this chapter tests will be carried out to ascertain whether there is a significant difference between the fracture intensities:

- in the hanging wall vs. footwall of the studied localities; an
- at localities with continuous shale smear vs. without, both in the footwall and hanging wall.

The data (Table 4.1) is assumed to be from a general population with normal distribution and is therefore suitable for parametric methods. Due to the large extent of cover at locality GNF1C, this locality was not included in the statistical analysis of the data. Some of the localities show areas of intensely fractured rocks. Where this is the case, fracture intensities of 100 have been used in the calculations.

Table 4.1: An overview of the key data that has been used in the statistical calculations.

Locality	Hanging wall/footwall	Mean (f/m)	Variance	n	Continuous shale smear
GNF1A	Footwall	54,5	184,6	17	Yes
	Hanging wall	39,6	99,9	18	Yes
GNF1B	Footwall	56,9	859,9	20	Yes
	Hanging wall	42,3	228,0	19	Yes
GNF1D	Footwall	61,1	416,5	17	Yes
	Hanging wall	40,2	31,5	22	Yes
GNF1E	Footwall	84,6	192,8	20	No
	Hanging wall	27,8	35,3	10	No

In order to test whether there is a significant difference in mean, the difference in variance has to be tested first. The variances of the samples is tested by using the Snedecor F-test (Davis, 2002). The outcome of the F-test decides which t-test function should be chosen in order to test the differences in mean (Davis, 2002). In both the Snedecor F-test and the Student t-test, a one-tail hypothesis was used.

Differences in fracture intensities between the hanging wall and footwall:

- Locality GNF1A: Since the H_0 of the F-test cannot be rejected, there must be assumed that the variances of the populations are similar ($F= 1.85 < F_{0.10}= 1.91$). The t-test show that the population`s means are significantly different, with 99%confidence ($t= 3.72 > t_{0.01}= 3.591$).
- Locality GNF1B: H_0 can be rejected with 99%confidence and the variances of the populations are significantly different ($F=3.77>F_{0.01} = 3.00$). The t-test show that the population`s means are significantly different, with 95% confidence ($t=1.918>t_{0.05}=1.69$)
- Locality GNF1D: H_0 can be rejected with 99% confidence, hence, the variances of the populations are significantly different ($F=13.22 > F_{0.01} =3.03$). The t-test show that the population`s means are significantly different, with 99. 5 confidence ($t=4.104>t_{0.005} = 2.74$.
- Locality GNF1E: H_0 can be rejected with 99% confidence and the variances of the populations are significantly different ($F=5.46>F_{0.01}=4.81$). The t-test show that the population`s means are significantly different, with 99. 5 % confidence ($t=15.65>t_{0.005}=2.763$).

The statistical analysis show that there is a significant difference between the fracture intensities in the footwall and the hanging wall at all the tested localities and that the fracture intensities of the footwall are significantly higher compared to the hanging wall.

Differences in fracture intensities of the footwall between localities with continuous shale smear (GNF1A, GNF1B and GNF1D) and without (GNF1E):

- Locality GNF1E compared with GNF1A: Since the H_0 of the F-test cannot be rejected, it must be assumed that the variances are similar ($F= 1.04 < F_{0.10}= 1.86$). The t-test show that the population`s means are significantly different,

with 99.5 % confidence (t= 6. 65 > $t_{0.005}$= 2.724), hence, the fracture intensities at locality GNF1E are significantly higher compared to GNF1A.

- Locality GNF1E compared with GNF1B: H_0 can be rejected with 99% confidence, hence the variances of the populations are significantly different (F=4. 46>$F_{0.01}$=3.00). The t-test show that the population`s means are significantly different, with 99.5 % confidence (t=3.818>$t_{0, 005}$=2.704), hence, there is a significant difference between GNF1B and GNF1E, where GNF1E show significantly higher fracture intensities in the footwall.
- Footwall at locality GNF1E compared with GNF1D: H_0 can be rejected with 90% confidence, hence the variances of the populations are significantly different (F=2, 16 >$F_{0.1}$=1, 86). The t-test show that the population`s means are significantly different, with 99, 5 % confidence (t=4.02>$t_{0.005}$=2.724). There can therefore be concluded that there is a significantly difference between GNF1E and GNF1D, where GNF1E show significantly higher fracture intensities in the footwall.

Differences in fracture intensities between localities with shale smear (GNF1A, GNF1B and GNF1D) and without (GNF1E) in the hanging wall:

- Hanging wall locality GNF1E compared with hanging wall GNF1A: F-test show that the variances of the populations are significantly different, and H_0 can be rejected with 90% confidence (F=2.83 >$F_{0.1}$=2.34). The t-test show that the populations means are significantly different, with 99.5 % confidence (t=3.91 > $t_{0.005}$=2.78). The test shows that the fracture intensities at GNF1A are significantly higher than GNF1E, hence higher intensities at the locality with continuous shale smear.
- Hanging wall locality GNF1E compared with hanging wall GNF1B: F-test show that the variances of the populations are significantly different, and H_0 can be rejected with 99% confidence (F=6.46 >$F_{0.01}$=4.81). The t-test show that the populations means are significantly different, with 99, 5 % confidence (t=3.67 > $t_{0.005}$=2.77). The test shows that the fracture intensities in the hanging wall at GNF1B are significantly higher than GNF1E, hence higher intensities on the locality with continuous shale smear.

- Hanging wall locality GNF1E compared with hanging wall GNF1D: F-test show that the variances of the populations are not significantly different, and H_0 cannot be rejected ($F=1.12 > F_{0,.01}=2.34$), hence have to be accepted. The t-test show that the population`s means are significantly different, with 99.5 % confidence ($t=5.69 > t_{0.005}=2.75$). The test shows that the fracture intensities in the hanging wall at GNF1D are significantly higher than GNF1E, hence higher intensities at the locality with continuous shale smear

The analysis presented shows that there is a significant difference between the footwall at the locality without continuous shale smear and the footwall at the localities with continuous shale smear. The trend in the hanging wall is rather the opposite; showing that the hanging wall at localities with continuous shale smears has significant higher fracture intensity compared to the locality without. The fracture intensities will be discussed further in the next chapter.

5. Discussion

5.1 Introduction

One of the aims of this study has been to investigate the role of shale smear in faults hosted in carbonate-shale sequences. How does shale smear influence the architecture, fracture pattern and sealing capacity of a fault zone? How does the fault zone evolve during increasing slip? Are the changes seen in the fault core and inner damage zone a result of increasing throw only, or does the presence or absence of shale smear make an impact? Could shale smear act as a "cushion" or "lubricant" that accommodates some of the strain, which in turns leads to less brittle deformation of the carbonates in the inner damage zone? The study reveals that the two studied faults exhibit several structural, geometrical and compositional variations within short distances along strike. The start of this chapter will discuss the evolution of the studied faults and their relationship to the block bounding fault (the Thal Fault). The fault growth and fault architecture in carbonate-shale sequences will be presented and discussed in order to elucidate the development of the fault core and inner damage zone. Field observations have also revealed the presence of fault related structures such as folding in the adjacent damage zone, and the mechanisms behind these structures will be discussed here. At the end of the chapter, all the observations of the fault core and inner damage zone will be used to assess the potential sealing capacity of the fault.

5.2 Regional evolution of GNF1 and GNF2

Several field- and modelling based studies on the evolution of faults suggest that individual faults grow by a systematic increase in maximum displacement and length and that faults grow as segments interact and become linked to form longer, continuous faults (e.g. Walsh and Watterson, 1988; Cartwright et al., 1995; Cowie, 1998; Wilson et al., 2009). The aspects of fault growth can be addressed where displacement and lengths of the fault can be reconstructed from information about the stratigraphy and landscape (e.g. Gawthorpe and Leeder, 2000; Gawthorpe et al., 2003). The formation and eventual breaching of relay zones is a common feature in fault zone evolution (e.g.Walsh et al., 2002). Studies have shown how the relay ramp, at a variety of scales, may evolve into fault-bounded lenses as two segments connect to form a single fault (e.g. Peacock and Sanderson, 1991; Faulkner et al., 2010).

GNF1, where most of the localities are situated, is observed to consist of several smaller fault segments. The throw plot of GNF1 (Fig. 3.3) shows the presence of several throw minima, both on the main fault and the overlapping segment. Throw minima generally indicate the

linkage point of originally individual faults (e.g. Peacock and Sanderson, 1996). Therefore, this indicates that the two overlapping faults of GNF1 consist of several presently hard-linked, smaller segments. The presence of only a single fault segment north of locality GNF1H, indicate that the two overlapping faults are hard-linked. Observations supporting the theory about the faults being hard-linked are seen in the northern part of the study area, where a large scale lens, shown as a zone of thickened fault rock is present. Although some authors have argued that branching of faults could result in a fault bounded lens as well (Childs et al., 2009), signs of this being a breached relay is also observed in the fracture patterns of the relay zone further south (Fig. 3.15), where the fractures are oriented in all directions. Several authors (e.g. Soliva et al., 2008) have shown that overlapping fault tips are associated with a rotation of the local stress field in the overlap zone, resulting in a variety of fracture orientations in the fault bounded relay zone. The large scale lens is therefore interpreted as a breached relay ramp, where originally individual faults have become a single, hard linked fault.

The small syn-rift basin in the study area is located close to the throw maxima of the GNF1, which may give an indication of the age relations of the fault. Several studies have used syn-rift stratigraphy to reconstruct the evolution of both intra block faults and border fault zones within the Hammam Faraun Fault Block (e.g. Gawthorpe et al., 2003; Young et al., 2003; Jackson et al., 2006a). Gawthorpe et al., (2003) argued that several of the intra block faults within the Hammam Faraun Fault Block were formed and grew by linkage of initially isolated fault segments, and that the intra block faults behaved as a single, hard linked segment during the deposition of the Nukhul Formation (Fig.5.1a). Some of the intra block faults were observed to have become inactive during Abu Zenima and Nukhul Formation times (Fig.5.1b) (Gawthorpe et al., 2003). The present day structural geometry of the Thal Fault Zone (Fig.5.1d) is similar to some of the intra block faults, but observations of the syn-rift stratigraphy however, indicate that the timing of the growth and linkage were quite different (Gawthorpe et al., 2003). The study of Gawthorpe et al. (2003) indicates that the Thal Fault were composed of long (4-8 km), isolated fault segments, and that the border fault zone did not become a major hard linked fault zone until late Rudeis Formation times (5.1c), in contrast to several of the intra-block faults which became hard-linked already in Nukhul Formation times (5.1b).

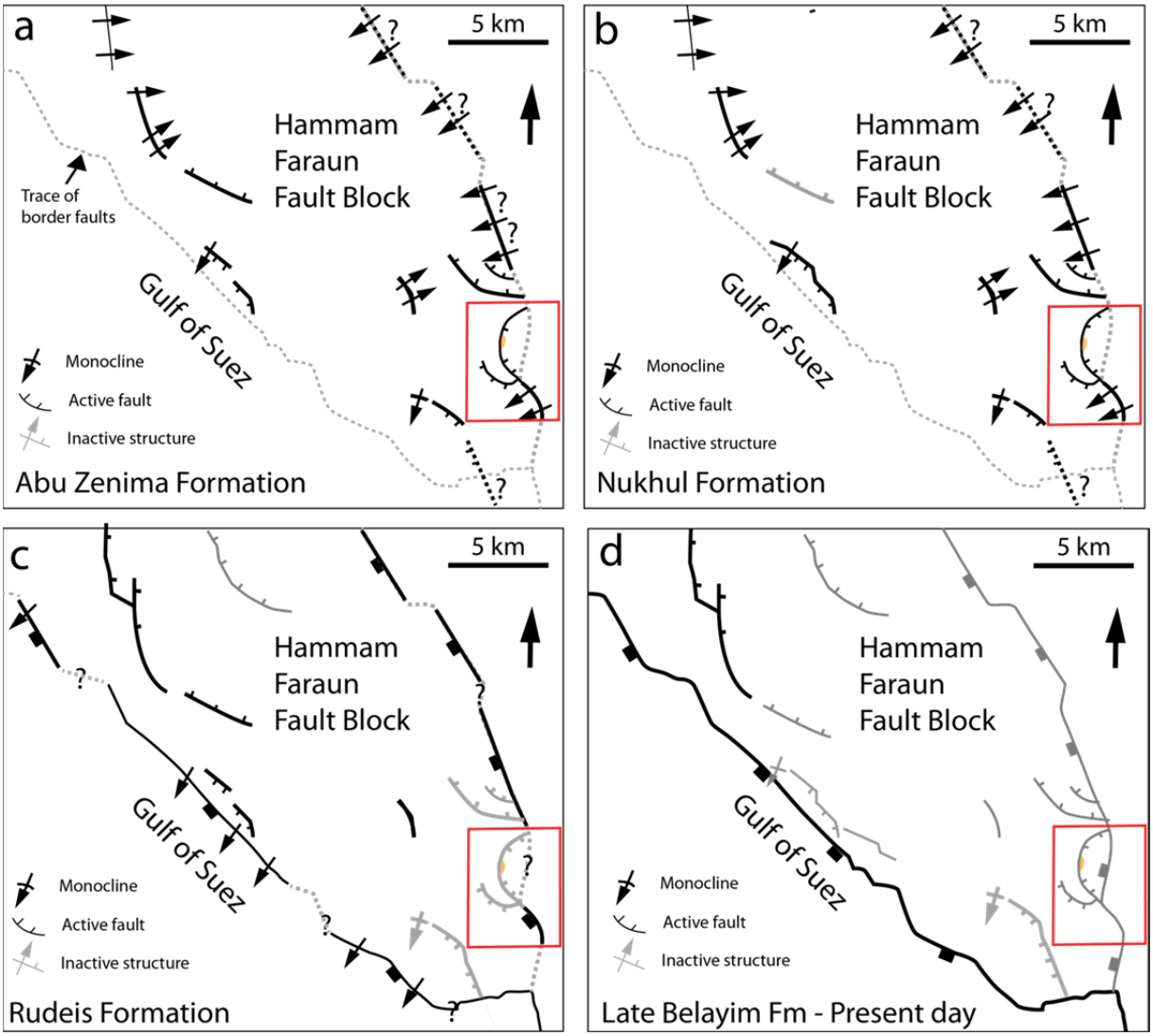

Fig. 5.1: Activity along the Thal Fault and presently studied fault segment, modified from Gawthorpe et al. (2003). a) The Hammam Faraun Fault Block and the studied faults during deposition of the Abu Zenima Formation. As indicated, the studied faults were active during this time and most likely acted as a single, hard-linked fault while the Abu Zenima Formation was deposited in the syn-rift basin (the orange area inside the red square). b) Due to the presence of the Nukhul Formation in the study area and signs of syn-sedimentary deposition, it is interpreted that the faults also were active during Nukhul Formation times. c) The absence of the Rudeis Formation in the syn-rift basin, and the general decreased activity on intra block faults in the study area, indicates that the studies faults died out between Nukhul and Rudeis Formation times. d) Present day structures, where the Thal Fault has linked up and formed a long, hard linked border fault zone

The small syn-rift basin in the study area displays formations interpreted to be of early syn-rift age (Abu Zenima Formation, 24-21.5 Ma and Nukhul Formation, 21.5-19.7 Ma). The slight thickening of the syn-rift sediments towards the GNF1 indicates syn-kinematic deposition, i.e. the sediments were deposited while GNF1 was still active. The presence of the syn-rift basin at the maximum throw of the fault, indicate that the GNF1 were established and most likely a hard linked fault during the early syn-rift stage (5.1a). The absence of any younger syn-rift sediments than the Nukhul Formation could either indicate that younger syn-

rift strata has been eroded away, or that the activity on the fault ceased shortly after deposition of the Nukhul Formation. The study of Gawthorpe et al., (2003)shows that some of the individual fault segments of the Thal Fault close to the studied faults were already active and propagating blindly during Abu Zenima Formation times, forming monocline structures (Fig. 5.1a). This is based on the structural relationship of the Thal Fault and early syn-rift sediments (Gawthorpe et al., 2003). The fault activity on the Thal Fault during Abu Zenima Formation times (5.1a) could indicate that GNF1 and GNF2 were already at this time connected to the Thal Fault. Based on 1) the age relations of the syn-rift sediments identified in the field area and the absence of any strata younger than the Nukhul Formation, 2) the connection with the Thal Fault and 3) the general evolution of the intra block faults in the study area (Gawthorpe et al., 2003), the studied faults are interpreted to have become inactive during Nukhul Formation times, when the fault activity re-localized to the Thal Fault.

5.3 Evolution of fault core and inner damage zone architecture in carbonate-shale sequences

Studies on fault zone evolution have the last decades made it increasingly apparent that faults cannot be regarded only as discrete slip surfaces, but rather as zones with a complex structure and geometry constituting deformed rocks (e.g.Caine et al., 1996; Childs et al., 2009; Wibberley and Shipton, 2010). The current study is no exception and as presented in the field descriptions in chapter 3, the internal structure and composition of the fault zone changes quite radically with only small changes in the throw. As pointed out in the introduction, the limitations of seismic resolution makes it inadequate to reveal the architecture and composition of fault core and damage zone features in the subsurface, which in turn are critical factors for understanding the fluid flow and the sealing capacity of faults. Therefore, field studies are essential to illuminate the connection between variations in displacement (detectable on seismic) and fault zone properties (generally not detectable on seismic) in order to understand the effect of faults on fluid flow in sub-surface carbonate reservoirs. To explain the growth of a fault zone in a carbonate-shale sequence in more detail and try to generalize the observations done in the area, the stages and architectural aspects of fault growth are discussed in the following, based on observations made in this study, in combination with previously published work.

5.3.1 Early stage of faulting: deformation at the fault tip and fault propagation folding

The early stages of fault growth inside the Hammam Faraun Fault Block are often associated with fault propagation folding, which is demonstrated by several studies (Sharp et al., 2000b; Khalil and McClay, 2002; Jackson et al., 2006b). These are produced by folding ahead of the propagating fault tip line. Processes and structures related to the early stages of faulting may be illuminated by observations from locality GNF2A in the study area, where the Thebes Formation is folded into a monoclinal fault propagation fold (Fig. 5.2). In the mechanically strong Thebes Formation, extension is accommodated by minor faulting, where both steep and low angle faults are observed (Fig.5.2). The low angle structures are most likely a result of rotation of an originally higher angle extensional fault. These features have also been observed by Jackson et al. (2006b), who studied early evolution of extensional faults in the northern part of the Red Sea rift. The deformation in the early stages of faulting seem to be controlled by both ductile and discrete brittle deformation mechanisms resulting in both folding and faulting of the Thebes Formation and folding of the Esna Formation (Fig. 5.2). A such monocline at locality GNF2A represents a partially breached fault propagation fold, where discrete brittle faults have localised in the mechanically strong and brittle limestone beds of the Thebes Formation ahead of the propagating fault tip.

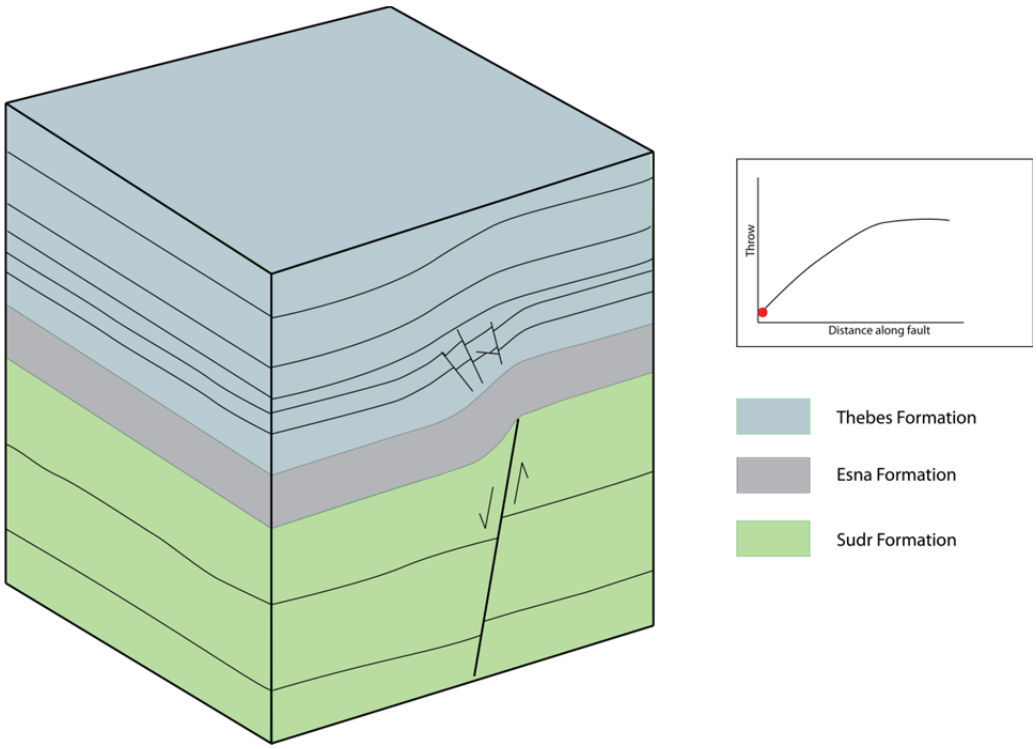

Fig. 5.2: Conceptual model of the early stages of fault growth in a carbonate-shale sequence, where a monocline is developed as a result of fault propagation folding.

5.3.2 Entrainment of shale, host rock lenses and fault rock lenses in the fault core

During continued propagation of any fault tip, layers affected by monoclinal folding (fault propagation folding) ahead of it (if present) are continually breached. As the fault develops, it allows the shale to be dragged into the fault zone by ductile deformation. The mechanisms and control on the development of shale smear is still debated, but the low shear strength of the clay is often seen as the main factor for shale smear development (e.g.Sperrevik et al., 2000), which allow the shale to deform in a ductile manner. The competency contrast between the clay and the surrounding material is also seen as an important factor for shale smear to develop, where clay, when it is less competent than the surrounding material, behaves in a ductile manner, which results in development of shale smear along the fault (Sperrevik et al., 2000). Although shearing and ductile deformation is normally seen as the main cause behind the development of shale smear in a fault, abrasion and injection of shale may result in shale smear as well (Lindsay et al., 1993; Møller-Pedersen and Koestler, 1997).

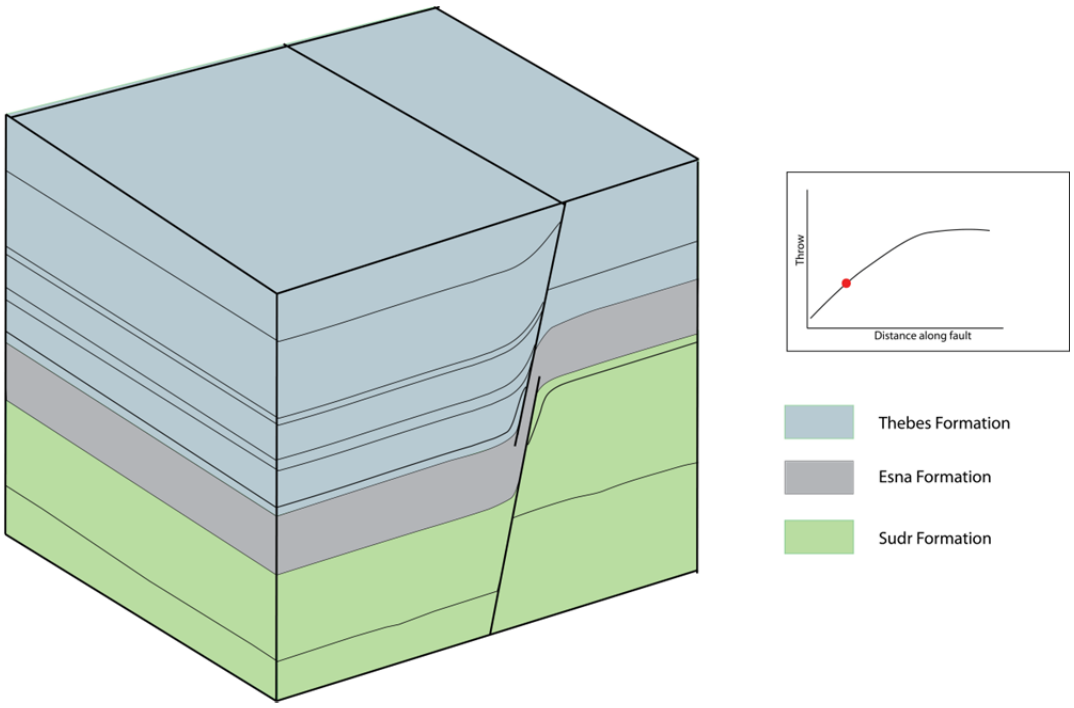

Fig. 5.3: As the throw increases on the fault, shale derived from the Esna Formation becomes entrained into the fault zone as shale smear. The hanging wall is dominated by folding, and lenses of fault rock becomes entrained into the fault zone as well.

Several localities in the study area have been observed with entrained, continuous shale smear. The shale smear is shown to be continuous with throw values up to 330 m (Fig. 3.18). As the key locality, displaying continuous shale smear, GNF1D is dominated by brittle deformation in terms of fractures and small faults, along with some ductile deformation observed as folding of the adjacent hanging wall (Fig.5.3). Along with thick, continuous shale smear derived from the Esna Formation, fault rock lenses have also been observed in the fault core (5.3).

The development of fault rock lenses and their relation to fluid flow in the fault zone has been investigated by several authors (e.g. Gabrielsen and Clausen, 2001; Lindanger et al., 2007; Bastesen, 2010). Their studies have shown that several mechanisms are active during the initiation and further development of fault core lenses, e.g. segment-linkage, asperity bifurcation, splitting by internal shear and tip-line coalescence. The fault related lenses investigated in this study appear to have been entrained into the fault core due to the rotation and dragging of limestone, marl and chalk beds by fault related folding. After the entrainment these beds are subsequently sheared off by secondary slip surfaces. This mechanism differs therefore from the above mentioned mechanism.

The presence of lenses may, depending on their properties, have implications for fluid flow. While host-rock lenses may increase cross-fault connectivity (if permeable), fault rock lenses (if low-permeable) may impede cross-fault connectivity (e.g. Childs et al., 1997; Knipe, 1997). The lenses present in the fault core have been interpreted as proto breccias. Calcite precipitations have been observed in the footwall lens, which could indicate paleo-fluid circulations in the lens. The high fraction of clay in the fault rock lenses and the low connectivity of the pores observed in photomicrographs indicate low permeability. The low permeability implies that the fault rock lenses here will most likely impede the cross-fault connectivity.

5.3.3 Relationship between fault throw, shale smear and fault core deformation

A discontinues shale membrane or the absence of shale is associated with an even higher throw (>350 m) (Fig. 5.3). This is exemplified by locality GNF1E. The fault zone changes drastically when the shale smear is absent, both in terms of increased deformation in the inner damage zone and thicker, more deformed fault rock lenses, which are derived from chalk beds of the Sudr Formation in the footwall. Chalk is known for a particular mechanical behaviour (Gaviglio et al., 2009), hence fault rock derived from chalk cannot necessarily be directly

compared with that of other carbonate rocks. Common features associated with deformation in chalk are dissolution, cementation, compaction and porosity reduction as a result of fluid induced digenesis (Gaviglio et al., 2009). Schroeder et al. (2006) showed that high levels of stress causes chalk to deform following an elastoplastic constitutive law, where deformation is dominated by pore collapse followed by hardening. Hardening and porosity reduction can also be formed due to fluid circulations and consequently dissolution and cementation of the pores. No porosity measurements of the lenses have been carried out, but investigation of the photomicrographs suggests a very low porosity (close to zero). No pronounced calcite cementation is observed in the outcrops or in the photomicrographs of the lenses. However, element mapping of some of the samples indicate high abundance of NaCl in the matrix of the fault rock, present as microcrystalline salt crystals. The low burial of the chalk (maximum 800 meters based on the above stratigrahpy) indicates that the Sudr Formation have experienced little compaction related to the overburden. This is also observed by investigating photomicrographs of undeformed samples from the Sudr Formation, where porosity is observed to be around 10-15 %.

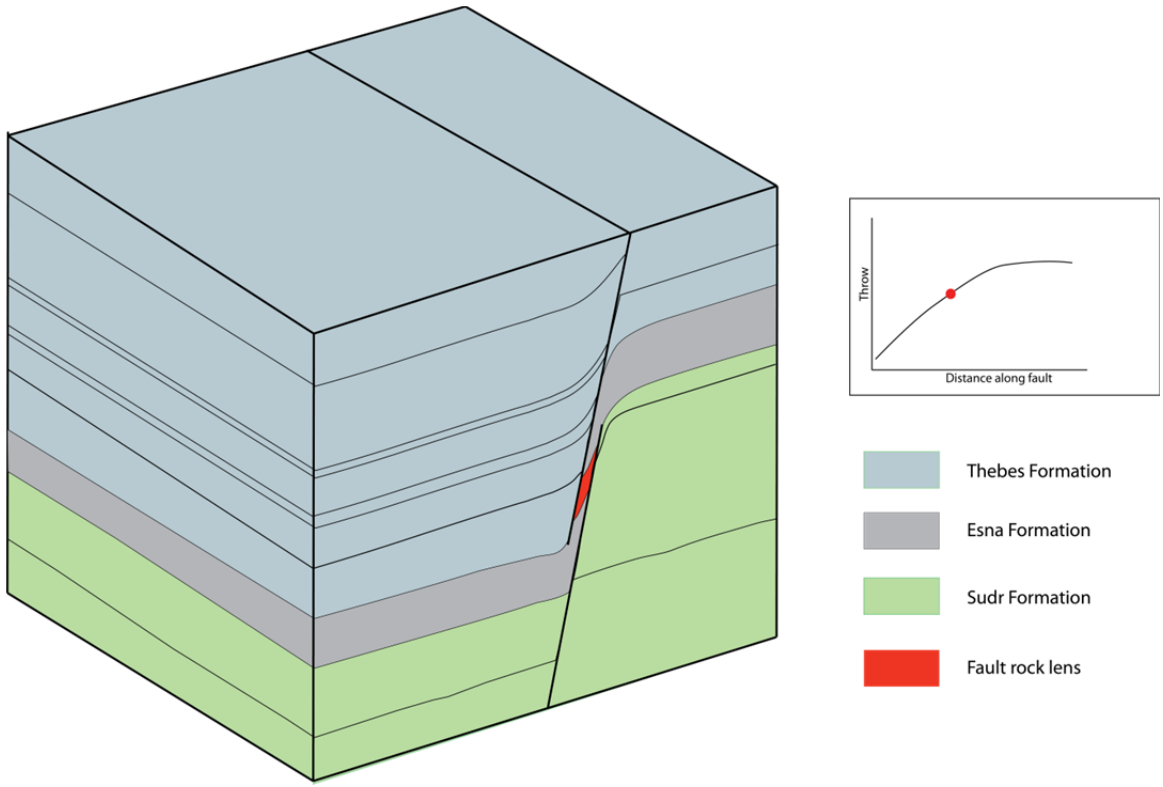

Fig 5.4: As the throw increases further, the shale smear becomes discontinuous. Highly deformed fault rock lenses derived from the Sudr Formation is present in the fault core, interpreted as an indurated breccia.

The enhanced concentration of NaCl could indicate fluid circulation with high NaCl content have flowed through the fault core. The present day low permeability and porosity of the fault rock lenses indicate that the NaCl is a sign of paleo fluid flow through the fault core. The observed low porosity and permeability of the sample, in a combination with the above mentioned evidence for paleo-fluid flow, suggests that whereas the fault core must have been a conduit for fluid circulation at an early stage, the present day properties of the fault core are a result of deformation at a later stage in the evolution of the fault. Due to the almost absence of calcite precipitation, low porosity and high clay content, this has been interpreted to be an indurated breccia, which has resulted from the enhanced stress acting on the fault core during slip. The obvious change in fault core composition could be a result of the absence of shale smear, since this may cause higher friction on the fault core due to no "lubrication" or "cushioning" in terms of shale smear. This could cause higher stress concentration in the fault core and result in higher strain accommodation in chalks and limestones.

5.3.4 Lateral fault segment linkage

In the northern part of the study area, a second fault segment is observed interacting with the main fault (Fig. 5.4). As presented in section 3.4.4, the damage zone between the overlapping faults is observed to be significantly more complex than the damage zone where only a single fault segment is present. The complexity is shown both in terms of elevated fracture intensities in this area and a wider range of orientations being present. The term relay-zone is often used when referring to rock volume between kinematically related fault segments (e.g. Cartwright et al., 1995). These rock bodies are zones where strain is transferred between overlapping fault segments through the folding of relay beds, which are ultimately breached when the overlapping fault physically link up (e.g. Peacock and Sanderson, 1991). Several studies have observed this complexity in relay zones and explained them as being related to local stress field modifications during interaction of overlapping fault segments (Kattenhorn et al., 2000; Soliva et al., 2008). A study on relay zones in carbonate rocks within the Hammam Faraun Fault Block indicates that fault linkage zones may, due to the increased intensity and complexity of fractures associated with such zones, represent localised conduits for increased fluid flow (Rotevatn and Bastesen, in press). Increased throw on overlapping faults will eventually cause breaching of the relay zone and form a hard-linked fault (e.g. Peacock and Sanderson, 1991; Childs et al., 2009). Breaching of the relay zone is seen at locality GNF1H, where a large scale lens is observed, interpreted to be remnants of a once existing soft-linked relay-ramp.

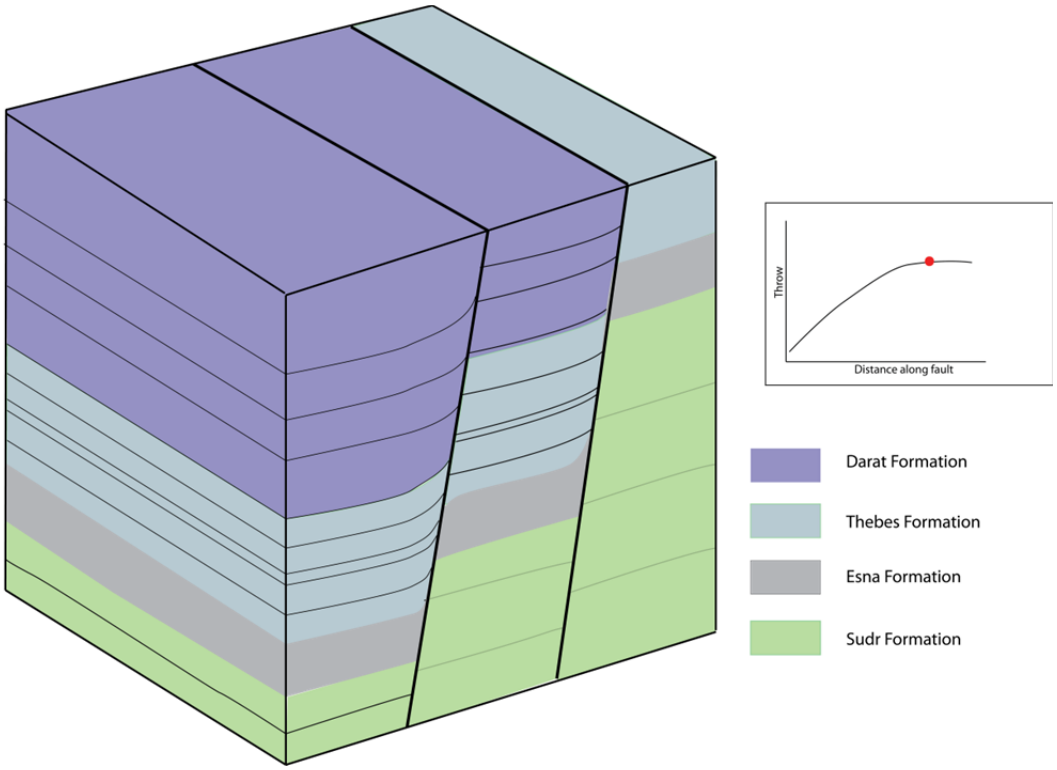

Fig 5.5: Observations from the study area indicates that the main fault becomes overlapped by a second fault, creating a relay zone in between. The relay zone show enhanced fracture intensities, where the fractures show no preferable orientation. Further north, a large scale lens is observed, indicating an established hard-link.

5.4 Damage zone variations and fault related folding

5.4.1 Fault related folding

Fault-related folds have received a lot of focus during the last decades, and several studies have highlighted the complex nature of these deformation features that can be observed both in the footwall and hanging wall of a fault zone (e.g Reches and Eidelman, 1995; Schlische, 1995; Khalil and McClay, 2002). As described in the previous chapter, several fault-related folds were observed in the study area and the mechanisms suggested to have formed these features will be discussed in the next section.

At several localities fault-parallel synclinal folds were observed in the adjacent hanging wall along the fault, with both steep (80 degrees) and more shallow (40 degrees) fold limbs. The extent of the synclines is observed to range from only the five-ten innermost meters (Locality GNF1A, B, C, E), up to 30 meters (GNF1D). Synclinal structures in the hanging wall, also termed normal drag by several authors (e.g. Reches and Eidelman, 1995;

Hesthammer and Fossen, 1998; Khalil and McClay, 2002; Rykkelid and Fossen, 2002), are commonly considered as a feature formed prior to faulting (fault propagation folds, which are subsequently breached as the fault tips propagates). The term normal drag is also used for folding related to other mechanisms. For instance, frictional drag, where strain hardening of the fault core results in drag folding in both the hanging wall and footwall, or lithology controlled drag where the folding is restricted to the ductile layers (Rykkelid and Fossen, 2002). Since the observed synclines in the study area are not restricted to the mechanical weak layers of the sequence, but rather affect all the layers in the hanging wall, the latter explanation of the normal drag folding can be ruled out.

The presence of partially breached monocline structures (interpreted as fault propagation folding previously in the discussion) in the study area (locality GNF2A), strongly suggests that breaching of fault propagation folds represent an important process for the formation of normal drag folding along the faults in the study area. However, the fact that the synclinal only extends in the innermost 5-30 meters at the different localities, indicate that the folding may also be controlled by strain hardening of the fault core. Since a fault propagation fold would, as Khalil and McClay (2002) shows, give a wider width of the synclinal in the adjacent hanging wall than what has been observed at most of the localities (except GNF1D), it could indicate that the folding also is a result of frictional drag along the fault plane.. The mechanisms behind the synclinal folding in the area are therefore interpreted to be a combination of frictional drag and breached fault propagation folds.

A different fold is observed in the northern part of the study area, as explained in section 3.4.4, where the layers in the hanging wall are folded toward the fault plane, creating an anticlinal fold. A change in dip on the fault plane is also observed, where steep dips in the upper part changes to a more shallow dip in the lower part, i.e. a listric fault geometry. Fault-parallel hanging wall anticlines such as this are often referred to as roll-over anticlines and are often seen in association with listric fault geometries (Reches and Eidelman, 1995). Movements along the curved fault plane tend to create a space problem which is accommodated by deformation of the hanging wall and folding into a rollover anticline. The listric shape of the fault plane is often seen in relation with an underlying weak layer, where the fault detaches and result in thinning and shearing of the weak layer (Williams and Vann, 1987). The faulted succession and the related rollover anticline is located close to the area where the thick shale layer of the Darat Formation (D1) is observed, which implies that the listric curvature of the fault plane is due to detachment into this underlying shale layer.

5.4.2 Evolution of the inner damage zone

The intensity and orientation of fractures have been recorded in the innermost damage zone of the different localities. In order to draw conclusions on the measured fracture intensities, statistical analysis was carried out (Chapter 4). The results show that there is a significant difference between the fracture intensities in the hanging wall and footwall, creating an asymmetrical deformation pattern around the fault core, where the footwall intensities is significant higher than the hanging wall intensities. Asymmetry in the damage zone may be related to irregularities along the fault trace, differences in rock properties or due to different stress conditions in the hanging wall and footwall during faulting (Knott et al., 1996; Berg and Skar, 2005). The evident difference in the mechanical properties of the Thebes and Sudr Formation is suggested to be one of the main reasons for the differences seen in the fracture intensities. While clay rich formations, such as the Thebes Formation (which consist of several intervals of shale), can accommodate a great amount of ductile strain, more homogenous limestone formations, such as Sudr Formation may fracture at much lower stresses. Evidence of mechanical differences internally in the Thebes Formation is also observed in the field, where fractures are observed to be stratabound, hence terminating at bed boundaries. This has been observed on fractures propagating in a limestone layer and dying out when reaching a shale layer for instance. Several authors have also shown that fracture spacing correlates with the bed thickness, where thicker beds will have higher fracture intensities (e.g. Ladeira and Price, 1981). This is especially seen where the competency contrast between the layers is high, for instance brittle limestone layers interbedded with ductile shale layers (Ladeira and Price, 1981).This might also be an explanation of the enhanced fracture intensities seen in the Sudr Formation, which is associated with much thicker bed-thicknesses compared to the Thebes Formation.

Statistical analysis of the fracture intensity data show that there is a significant difference between localities with continuous shale smear and without, but the difference is restricted to the footwall. This has been examined by comparing the fracture intensities at locality GNF1E (no continuous shale smear detected) with localities GNF1A, B, C, D (continuous shale smear present). The fact that the significant difference is restricted to the footwall could be due to the different parts of the Thebes Formation crop out at the different localities. While the middle Sudr Formation is exposed at every locality in the footwall, consisting of massive chalk beds, all the different parts of the Thebes Formation is successively displayed in the hanging wall as the throw increases. The fracture intensities at the different localities could therefore be a result of changes in the Thebes Formation, which

indicate that the intensities are hard to compared, since the mechanical properties of the different layers might differ, due to different thicknesses and lithologies at the different localities. However, given the homogeneous nature of the Sudr Formation in the footwall, the significant difference in fracture intensities where shale smear is present versus where it is absent, it is not thought to be related to differences in mechanical properties.

One reason for the elevated fracture intensities might simply be related to the increase in throw from the locality with continuous shale smear to the locality without, where the increased throw has caused increased fracturing in the inner damage zone. However, the fact that the localities are only situated about 200 meters from each other and that the difference in throw is only approximately 30 meters, indicates that this significant difference in fracture intensity is not related to an increase in fault throw alone, but rather related to the absence of continuous shale smear. This indicates that where shale smear is present, some proportion of the strain is accommodated in the shale layer in a ductile manner. Contrarily, along the part of the fault where shale smear is absent, strain is more widely distributed and accommodated in a more brittle manner, affecting the core as well as the inner damage zone. The absence of shale is probably also associated with an increased friction along the slip surface. This results in a higher fracture intensities and increased brittle crushing and compaction of the fault core and inner damage zone of the footwall limestone layers.

5.5 Comments on the use of Shale Smear Factor on larger (> 100 m throw) faults

The result presented in this thesis may shed some light on the use of shale smear factor in fault seal analysis. The shale smear factor was first introduced by Lindsay et al., (1993) who studied small faults (< 15 m throw), predominantly in sandstone-shale sequences. To assess the likelihood of continuous smear in the fault zone, they introduced a shale smear factor, which is given by the fault throw divided by the vertical thickness (Lindsay et al., 1993). They concluded that with a shale smear factor ≤7, a continuous shale smear can be expected, while if it is ≤11, it is only probable to have a continuous shale smear in the fault zone. Despite the fact that the shale smear factor, as described in Lindsay et al., (1993), is based on empirical data from small faults (< 15 m throw), it is commonly used by workers who wants to address the likelihood of continuous shale smear along larger faults (e.g. Knipe, 1997; Sperrevik et al., 2002), assuming that the shale smear factor is not affected by scale

The calculations on shale smear factor from the current study, show that with a shale smear factor ≤ 6.5, continuous smear is observed in the fault zone, while with a SSF > 6.5, continuous shale smear is absent. The disparity of the shale smear calculated in the current study and shale smear factor derived from Lindsay et al., (1993) has also been seen by other authors investigating shale smear factor on larger faults (e.g. Aydin and Eyal, 2002; Færseth, 2006), and the current study add weight to this view, and concludes that shale smear factors derived from small faults cannot be used to predict shale smear continuity on larger faults, and that a different threshold should be used when dealing with large (>100 m) faults. The calculated shale smear factor for this study, based on one fault only, should not be regarded as an attempt to introduce a new threshold to predict shale smear continuity. However, this study supports the views of Færseth (2006) that the use of shale smear factor in fault seal analysis may have limited applicability to large faults. Therefore, the use of shale smear factor should be treated with caution when trying to address the likelihood of smear on larger faults. More empirical studies of the relationship between shale bed thicknesses, throw and continuity of shale smear for larger faults would be necessary to further develop the use of shale smear factor to predict smear on larger faults.

5.6 A model for the fault zone permeability structure

A secondary objective of the study has been to investigate the sealing potential of the GNF1, by using observations of the fault core and damage zone, and to use this to extract some generic lessons on the permeability structure of faults in carbonate rocks. As mentioned in the introduction, tight faults in carbonate rocks may act as a combined conduit-barrier system where the fault core usually (but not always) act as a seal, while the damage zone may act as a conduit due to the high density of fractures which is often associated with this part of the fault zone (Agosta and Aydin, 2006; Micarelli et al., 2006; Bastesen et al., 2009). Although no petrophysical measurements have been carried out in this study in regards to permeability and porosity in the fault core, the descriptions of the localities and thin sections may give an indication of the permeability structure of the GNF1.

Fault seal may arise from the juxtaposition of reservoir units against non-reservoir units or the presence of a low permeable membrane seal (Færseth, 2006). There are three mechanisms that are believed to form a sealing membrane along faults: these include cataclasis, cementation and shale smear (Lindsay et al., 1993; Knipe, 1997).

As pointed out in the previous section, the presence of continuous shale smear is associated with throw values up to 330 m. The presence of shale smear in the fault core will act as a sealing membrane due to the low permeability which is generally associated with shale. When the throw values exceed 330 meters, the shale smear in the fault zone is observed to get thinner and eventually become discontinuous. As seen in the previous part of the discussion, the point at which the shale smear becomes discontinuous is associated with a radical change in the fault core composition (Fig.5.6). At this stage, the fault core is comprised of a thick zone of breccia derived from the Sudr Formation. The breccia, which displays low porosity and presumably low permeability due to the high fraction of shale, is likely to act as a sealing membrane in the same way as the when the shale smear govern the fault core. Agosta et al., (2007) did modelling in regards to the sealing potential of fault cores that were fine grained, non-cemented and of low porosity and permeability. They showed that the cores presented in their study could seal up to as much as 77 m and 140 m of gas and oil respectively. The similarities of the fault core presented at the stage of which shale smear becomes discontinuous and the fault core modelled by Agosta et al., (2007) is an indication that the fault core will act as a seal in regard to fluid flow. As the throw increases, shale smear derived from the Darat Formation becomes entrained into the fault zone (Fig.5.6), acting the same way as the Esna Formation, increasing the sealing potential of the fault.

Previous studies have shown that host rock lenses may create pathways vertical and cross- fault fluid flow, depending on their degree of deformation. The lenses observed at some of the localities may therefore represent potential leakage points. The lenses present show some degree of deformation, but still with some of the porosity left. Calcite cement has been observed in the footwall lens, suggesting that circulation of fluids at a previous stage. Due to the present low permeability of both the lenses, it is concluded that in their present state they will reduce fluid flow.

The fracture pattern of the inner damage zone at the studied localities, displays high intensities in the footwall, especially where the shale smear becomes discontinuous (Fig.5.6). The damage zone is dominated by opening mode and shear fractures with thick calcite cement. The damage zone shows an asymmetry between footwall and hanging wall, where the footwall, due to the associated higher fracture intensities, is more permeable than the hanging wall. The fracture pattern changes where the fault becomes segmented, displaying enhanced fracture intensities and a wide range of orientations in the relay zone between the overlapping fault segments. The study of Agosta et al., (2007) also modelled the effect of the intensely fractured damage zone, which consisted of several sets of opening mode fractures (joints and

veins) to fluid flow. The results showed that the damage zone of the fault formed a conduit in relation to fluid flow. Recent studies on relay zones have also shown that the associated fracture intensities and diversity of orientations may represent a localized conduit where fluid flow is increased both across and vertically along faults (Rotevatn and Bastesen, in press). The presence of a relay zone in the study area and the associated diversity of orientations indicate that that the relay zone in the study area would act as a localized conduit in relation to fluid flow.

The current study, based on the field observations, indicate that the GNF1 would act as a combined conduit-barrier system in relation to fluid flow.

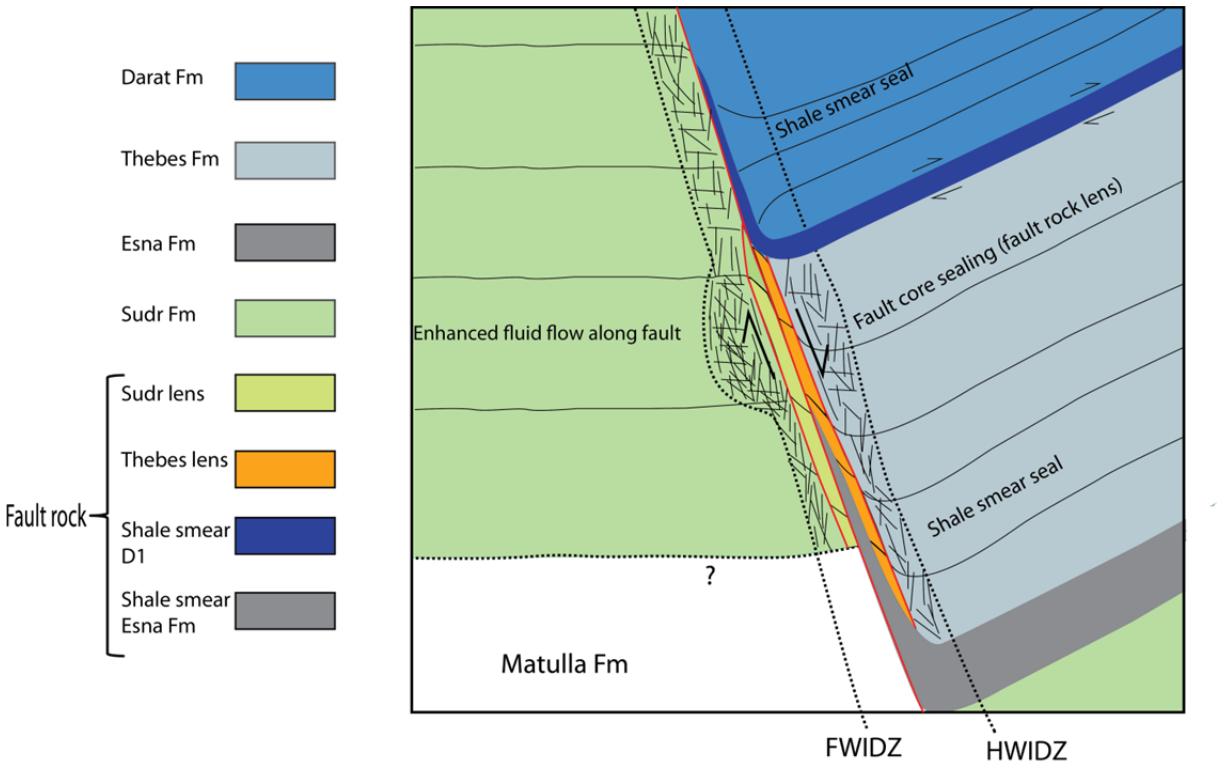

Fig. 5.6: The figure summarise the observations made in regards to fault core composition and damage zone characteristics for the GNF1. The presence of shale smear and impermeable fault rock lenses indicate that the fault will act as a seal in terms of fluid flow. The enhanced fracture intensities seen in the inner damage zone, especially in the footwall and especially where shale smear is absent, is seen to enhance the fluid flow along the fault. The figure is not to scale.

6. Conclusions

The current study has been focusing on the variability and co-dependence of throw and shale smear and the associated changes in fault zone composition and geometry. The following conclusions are drawn:

- The findings of this study suggest that the development of the fault core is affected by the presence or absence of shale smear, in the sense that the shale smear act as a "cushion", accommodating ductile strain. This is seen by the presence of a significantly more deformed fault core and inner damage zone where shale smear is absent, in contrast to only minor brittle deformation where the shale smear is present.

- It is also concluded from this study that the absence of shale smear in the fault zone is associated with enhanced fracture intensities in the footwall. The restriction of this effect to the footwall can be explained by a difference in the mechanical properties between the hanging wall and footwall host rock.

- The observations of fault core and inner damage zone suggest that the fault zone will act as a combined barrier-conduit in relation to fluid flow. The presence of shale smear, highly deformed, impermeable breccias in the fault core along the fault, demonstrates that the sealing potential of the studied fault is relatively high. The presence of large fractures and intensely fractured foot wall, especially where shale smear is absent and in the overlap zone, suggest that this part of the fault will act as a conduit, increasing both the lateral and vertical permeability.

- The calculated shale smear factor for the area reveals that with a shale smear factor above 6.5, the shale smear becomes discontinuous. The calculated shale smear factor for the study area is according to other studies on larger faults, concluding that the shale smear factor threshold derived from small faults cannot be used to predict shale smear continuity on larger faults, or at least be used with caution.

7. References

Agosta, F., Aydin, A., 2006. Architecture and deformation mechanism of a basin-bounding normal fault in Mesozoic platform carbonates, central Italy. Journal of Structural Geology 28, 1445-1467.

Agosta, F., Prasad, M., Aydin, A., 2007. Physical properties of carbonate fault rocks, fucino basin (Central Italy): implications for fault seal in platform carbonates. Geofluids 7, 19-32.

Anderson, E.M., 1951. The Dynamics of faulting (2nd ed), Edinburgh.

Aydin, A., 2000. Fractures, faults, and hydrocarbon entrapment, migration and flow. Marine and Petroleum Geology 17, 797-814.

Aydin, A., Eyal, Y., 2002. Anatomy of a normal fault with shale smear: Implications for fault seal. Aapg Bulletin 86, 1367-1381.

Bastesen, E., 2010. Facies composition and scaling of extensional faults in sedimentary rocks and its application of fault zones. University of Bergen, Bergen.

Bastesen, E., Braathen, A., 2010. Extensional faults in fine grained carbonates - analysis of fault core lithology and thickness-displacement relationships. Journal of Structural Geology 32, 1609-1628.

Bastesen, E., Braathen, A., Nottveit, H., Gabrielsen, R.H., Skar, T., 2009. Extensional fault cores in micritic carbonate - Case studies from the Gulf of Corinth, Greece. Journal of Structural Geology 31, 403-420.

Bastesen, E., Rotevatn, A., in press. Evolution and structural style of relay zones in layered limestone shale sequences: Insights from the Hammam Faraun Fault Block, Suez Rift, Egypt. Journal of geological society of London.

Berg, S.S., Skar, T., 2005. Controls on damage zone asymmetry of a normal fault zone: outcrop analyses of a segment of the Moab fault, SE Utah. Journal of Structural Geology 27, 1803-1822.

Boggs, S., 2001. Principles of sedimentology and stratigraphy. Prentice Hall, Upper Saddle River, N.J.

Bosworth, W., Huchon, P., McClay, K., 2005. The Red Sea and Gulf of Aden basins. J. Afr. Earth Sci. 43, 334-378.

Braathen, A., Osmundsen, P.T., Gabrielsen, R.H., 2004. Dynamic development of fault rocks in a crustal-scale detachment: An example from western Norway. Tectonics 23.

Braathen, A., Tveranger, J., Fossen, H., Skar, T., Cardozo, N., Sernshaug, S.E., Bastesen, E., Sverdrup, E., 2009. Fault facies and its application to sandstone reservoirs. Aapg Bulletin 93, 891-917.

Caine, J.S., Evans, J.P., Forster, C.B., 1996. Fault zone architecture and permeability structure. Geology 24, 1025-1028.

Cartwright, J.A., Trudgill, B.D., Mansfield, C.S., 1995. Fault growth by segment linkage - An explanation for scatter in maximum displacement and trace length data from the Canyonlands graben of SE Utah. Journal of Structural Geology 17, 1319-1326.

Chester, F.M., Logan, J.M., 1987. Composite planar fabric of gouge from the Punchbowl fault, California. Journal of Structural Geology 9, 621-634.

Childs, C., Manzocchi, T., Walsh, J.J., Bonson, C.G., Nicol, A., Schoepfer, M.P.J., 2009. A geometric model of fault zone and fault rock thickness variations. Journal of Structural Geology 31, 117-127.

Childs, C., Walsh, J.J., Watterson, J., 1997. Complexity in fault zone structure and implications for fault seal prediction, in: Møller-Pedersen, P., Koestler, A.G. (Eds.), Norwegian Petroleum Society Special Publications. Elsevier, pp. 61-72.

Cochran, J., 1983. A model for development of Red Sea. Aapg Bulletin 67, 41-69.

Cowie, P.A., 1998. A healing-reloading feedback control on the growth rate of seismogenic faults. Journal of Structural Geology 20, 1075-1087.

Davis, G.H., Reynolds, S.J., 1996. Structural geology of rocks and regions. John Wiley, New York.

Davis, J.C., 2002. Statistics and data analysis in geology. J. Wiley, New York.

Dunham, R.J., 1962. Classification of carbonate rocks according to depositional texture, in: W.E., H. (Ed.), Classification of carbonate rocks. Am. Assoc. Petrol. Geol. Mem 1, pp. 108-121.

Faulkner, D.R., Jackson, C.A.L., Lunn, R.J., Schlische, R.W., Shipton, Z.K., Wibberley, C.A.J., Withjack, M.O., 2010. A review of recent developments concerning the structure, mechanics and fluid flow properties of fault zones. Journal of Structural Geology 32, 1557-1575.

Ferrill, D.A., Morris, A.P., 2008. Fault zone deformation controlled by carbonate mechanical stratigraphy, Balcones fault system, Texas. Aapg Bulletin 92, 359-380.

Ferrill, D.A., Morris, A.P., McGinnis, R.N., Smart, K.J., Ward, W.C., 2011. Fault zone deformation and displacement partitioning in mechanically layered carbonates: The Hidden Valley fault, central Texas. Aapg Bulletin 95, 1383-1397.

Færseth, R.B., 2006. Shale smear along large faults: continuity of smear and the fault seal capacity. J. Geol. Soc. 163, 741-751.

Gabrielsen, R.H., Clausen, J.A., 2001. Horses and duplexes in extensional regimes: A scale-modeling contribution, in: Koyi, H., Mancktelow, N.S. (Eds.), Tectonic modeling: a volume in honor of Hans Ramberg. The Society, Boulder, Colo., pp. IX, 276 s.

Garfunkel, Z.B., Y., 1977. Tectonics of the Suez Rift. Geological Survey of Israel Bulletin 71, 1-41.

Gaviglio, P., Bekri, S., Vandycke, S., Adler, P.M., Schroeder, C., Bergerat, F., Darquennes, A., Coulon, M., 2009. Faulting and deformation in chalk. Journal of Structural Geology 31, 194-207.

Gawthorpe, R.L., Jackson, C.A.L., Young, M.J., Sharp, I.R., Moustafa, A.R., Leppard, C.W., 2003. Normal fault growth, displacement localisation and the evolution of normal fault populations: the Hammam Faraun fault block, Suez rift, Egypt. Journal of Structural Geology 25, 883-895.

Gawthorpe, R.L., Leeder, M.R., 2000. Tectono-sedimentary evolution of active extensional basins. Basin Research 12, 195-218.

Gupta, S., Underhill, J.R., Sharp, I.R., Gawthorpe, R.L., 1999. Role of fault interactions in controlling synrift sediment dispersal patterns: Miocene, Abu Alaqa Group, Suez Rift, Sinai, Egypt. Basin Research 11, 167-189.

Hesthammer, J., Fossen, H., 1998. The use of dipmeter data to constrain the structural geology of the Gullfaks Field, northern North Sea. Marine and Petroleum Geology 15, 549-573.

Jackson, C.A.L., Gawthorpe, R.L., Leppard, C.W., Sharp, I.R., 2006a. Rift-initiation development of normal fault blocks: insights from the Hammam Faraun fault block, Suez Rift, Egypt. J. Geol. Soc. 163, 165-183.

Jackson, C.A.L., Gawthorpe, R.L., Sharp, I.R., 2002. Growth and linkage of the East Tanka fault zone, Suez rift: structural style and syn-rift stratigraphic response. J. Geol. Soc. 159, 175-187.

Jackson, C.A.L., Gawthorpe, R.L., Sharp, I.R., 2006b. Style and sequence of deformation during extensional fault-propagation folding: examples from the Hammam Faraun and El-Qaa fault blocks, Suez Rift, Egypt. Journal of Structural Geology 28, 519-535.

Kattenhorn, S.A., Aydin, A., Pollard, D.D., 2000. Joints at high angles to normal fault strike: an explanation using 3-D numerical models of fault-perturbed stress fields. Journal of Structural Geology 22, 1-23.

Khalil, S.M., McClay, K.R., 2002. Extensional fault-related folding, northwestern Red Sea, Egypt. Journal of Structural Geology 24, 743-762.

Knipe, R.J., 1997. Juxtaposition and seal diagrams to help analyze fault seals in hydrocarbon reservoirs. Aapg Bulletin-American Association of Petroleum Geologists 81, 187-195.

Knott, S.D., Beach, A., Brockbank, P.J., Brown, J.L., McCallum, J.E., Welbon, A.I., 1996. Spatial and mechanical controls on normal fault populations. Journal of Structural Geology 18, 359-372.

Kuss, J.S., C.; Gietl, R. , 2000. Carbonate Platform to Basin Transition along an Upper Cretaceous to Lower Tertiary Syrian Arc Uplift, Galala Plateaus, Eastern Desert of Egypt. GeoArabia 5.

Ladeira, F.L., Price, N.J., 1981. Relationship between fracture spacing and bed thickness Journal of Structural Geology 3, 179-&.

Leppard, C.W., Gawthorpe, R.L., 2006. Sedimentology of rift climax deep water systems; Lower Rudeis Formation, Hammam Faraun Fault Block, Suez Rift, Egypt. Sedimentary Geology 191, 67-87.

Lindanger, M., Gabrielsen, R.H., Braathen, A., 2007. Analysis of rock lenses in extensional faults. Norw. J. Geol. 87, 361-372.

Lindsay, N.G., Murphy, F.C., Walsh, J.J., Watterson, J., 1993. Outcrop studies of shales smears on fault surfaces., in: Flint, S.S.B., I.D. (Ed.), The Geological Modelling of Hydrocarbon Reservoirs and Outcrop Analogues. International Association of Sedimentologists, pp. 113-123.

Lyberis, N., 1988. Tectonic evolution of the Gulf of Suez and the Gulf of Aqaba. Tectonophysics 153, 209-220.

Mazzullo, S.J., 2004. Overview of porosity evolution in carbonate reservoirs. Kansas Geological Society Bulletin 79, 20-28.

Micarelli, L., Benedicto, A., Wibberley, C.A.J., 2006. Structural evolution and permeability of normal fault zones in highly porous carbonate rocks. Journal of Structural Geology 28, 1214-1227.

Moustafa, A.R., 1993. Structural characteristics and tectonic evolution of the east-margin blocks of the Suez Rift. Tectonophysics 223, 381-399.

Moustafa, A.R., 1996. Structural setting and tectonic evolution of the northern Hammam Faraun block (Wadi Wasit Wadi Wardan area), eastern side of the Suez rift. J. Univ. Kuwait-Sci. 23, 105-132.

Moustafa, A.R., 2004. Explanatory Notes for the Geologic Maps of the Eastern Side of the Suez Rift (Western Sinai Peninsula), AAPG/Datapages GIS Series, Cairo.

Moustafa, A.R., Abdeen, M.M., 1992. Structural setting of the Hammam Faraun Block, eastern side of the Suez Rift J. Univ. Kuwait-Sci. 19, 291-309.

Møller-Pedersen, P., Koestler, A.G., 1997. Hydrocarbon seals: importance for exploration and production. Elsevier, Amsterdam, pp. XII, 250 s.

NasaScienceLibrary, 2012. Shuttle Image of Red Sea & Sinai Peninsula, in: Library, N.S.P. (Ed.).

Patton, T.L., Moustafa, A.R., Nelson, R.A., Abdine, S.A., 1994. Tectonic Evolution and Structural Setting of the Suez Rift, in: Landon, S.M. (Ed.), Interior Rift Basins. The American Association of Petroleum Geologists, Tulsa, Oklahoma.

Peacock, D.C.P., Sanderson, D.J., 1991. Displacements, segment linkage and relay ramps in normal-fault zones. Journal of Structural Geology 13, 721-&.

Peacock, D.C.P., Sanderson, D.J., 1996. Effects of propagation rate on displacement variations along faults. Journal of Structural Geology 18, 311-320.

Reches, Z., Eidelman, A., 1995. Drag along faults. Tectonophysics 247, 145-156.

Rotevatn, A., Bastesen, E., in press. Fault linkage and damage zone architecture in tight carbonate rocks in the Suez Rift (Egypt): implications for permeability structure along segmented normal faults. Journal of geological society of London.

Rykkelid, E., Fossen, H., 2002. Layer rotation around vertical fault overlap zones: observations from seismic data, field examples, and physical experiments. Marine and Petroleum Geology 19, 181-192.

Samuel, M.D., Ismail, A.A., Akarish, A.I.M., Zaky, A.H., 2009. Upper Cretaceous stratigraphy of the Gebel Somar area, north-central Sinai, Egypt. Cretaceous Research 30, 22-34.

Scheibner, C., Kuss, J., Marzouk, A.M., 2000. Slope sediments of a Paleocene ramp-to-basin transition in NE Egypt. Int. J. Earth Sci. 88, 708-724.

Schlische, R.W., 1995. Geometry and origin of fault-related folds in extensional settings Aapg Bulletin-American Association of Petroleum Geologists 79, 1661-1678.

Schroeder, C., Gaviglio, P., Bergerat, F., Vandycke, S., Coulon, M., 2006. Faults and matrix deformations in chalk: contribution of porosity and sonic wave velocity measurements. Bulletin De La Societe Geologique De France 177, 203-213.

Sharp, I.R., Gawthorpe, R.L., Armstrong, B., Underhill, J.R., 2000a. Propagation history and passive rotation of mesoscale normal faults: implications for synrift stratigraphic development. Basin Research 12, 285-+.

Sharp, I.R., Gawthorpe, R.L., Underhill, J.R., Gupta, S., 2000b. Fault-propagation folding in extensional settings: Examples of structural style and synrift sedimentary response from the Suez rift, Sinai, Egypt. Geological Society of America Bulletin 112, 1877-1899.

Sibson, R.H., 1977. Fault rocks and fault mechanisms. Journal of the Geological Society of London, 191-213.

Soliva, R., Benedicto, A., Schultz, R.A., Maerten, L., Micarelli, L., 2008. Displacement and interaction of normal fault segments branched at depth: Implications for fault growth and potential earthquake rupture size. Journal of Structural Geology 30, 1288-1299.

Sperrevik, S., Faerseth, R.B., Gabrielsen, R.H., 2000. Experiments on clay smear formation along faults. Petrol. Geosci. 6, 113-123.

Sperrevik, S., Gillespie, P.A., Fisher, Q.J., Halvorsen, T., Knipe, R.J., 2002. Empirical estimation of fault rock properties, in: Andreas, G.K., Robert, H. (Eds.), Norwegian Petroleum Society Special Publications. Elsevier, pp. 109-125.

Verhaert, G., Muchez, P., Keppens, E., Sintubin, M., 2009. Fluid impact and spatial and temporal evolution of normal faulting in limestones. A case study in the Burdur-Isparta region (SW Turkey) Geologica Belgica 12, 59-73.

Walsh, J.J., Nicol, A., Childs, C., 2002. An alternative model for the growth of faults. Journal of Structural Geology 24, 1669-1675.

Walsh, J.J., Watterson, J., 1988. Analysis of the relationship between displacements and dimensions of faults Journal of Structural Geology 10, 239-247.

Wibberley, C.A.J., Shipton, Z.K., 2010. Fault zones: A complex issue. Journal of Structural Geology 32, 1554-1556.

Wibberley, C.A.J., Yielding, G., Di Toro, G., 2008. Recent advances in the understanding of fault zone internal structure: a review. Geological Society, London, Special publications 2008 299, 5-33.

Williams, G., Vann, I., 1987. The geometry of listric normal faults and deformation in their hangingwalls. Journal of Structural Geology 9, 789-795.

Wilson, P., Gawthorpe, R.L., Hodgetts, D., Rarity, F., Sharp, I.R., 2009. Geometry and architecture of faults in a syn-rift normal fault array: The Nukhul half-graben, Suez rift, Egypt. Journal of Structural Geology 31, 759-775.

Wise, D.U., Dunn, D.E., Engelder, J.T., Geiser, P.A., Hatcher, R.D., Kish, S.A., Odom, A.L., Schamel, S., 1984. Fault-related rocks- suggestions for terminology. Geology 12, 391-394.

Yielding, G., Freeman, B., Needham, D.T., 1997. Quantitative fault seal prediction. Aapg Bulletin-American Association of Petroleum Geologists 81, 897-917.

Young, M.J., Gawthorpe, R.L., Sharp, I.R., 2000. Sedimentology and sequence stratigraphy of a transfer zone coarse-grained delta, Miocene Suez Rift, Egypt. Sedimentology 47, 1081-1104.

Young, M.J., Gawthorpe, R.L., Sharp, I.R., 2002. Architecture and evolution of syn-rift clastic depositional systems towards the tip of a major fault segment, Suez Rift, Egypt. Basin Research 14, 1-23.

Young, M.J., Gawthorpe, R.L., Sharp, I.R., 2003. Normal fault growth and early syn-rift sedimentology and sequence stratigraphy: Thal Fault, Suez Rift, Egypt. Basin Research 15, 479-502.